(21) Pierschbacher, M. D., and Ruoslahti, E. (1984) Variants of the cell recognition site of fibronectin that retain attachment-promoting activity. *Proc. Natl. Acad. Sci. U.S.A. 81*, 5985−5988.
(22) Dechantsreiter, M. A., Planker, E., Mathä, B., Lohof, E., Hölzemann, G., Jonczyk, A., Goodman, S. L., and Kessler, H. (1999) *N*-Methylated cyclic RGD peptides as highly active and selective $\alpha_v\beta_3$ integrin antagonists. *J. Med. Chem. 42*, 3033−3040.
(23) Allen, T. M. (2002) Ligand-targeted therapeutics in anticancer therapy. *Nat. Rev. 2*, 750−763.
(24) Kim, W. J., Yockman, J. W., Lee, M., Jeong, J. H., Kim, Y.-H., and Kim, S. W. (2005) Soluble *Flt-1* gene delivery using PEI-*g*-PEG-RGD conjugate for anti-angiogenesis. *J. Controlled Release 106*, 224−234.
(25) Kim, W. J., Yockman, J. W., Jeong, J. H., Christensen, L. V., Lee, M., Kim, Y.-H., and Kim, S. W. (2006) Anti-angiogenic inhibition of tumor growth by systemic delivery of PEI-*g*-PEG-RGD/pCMV-sFlt-1 complexes in tumor-bearing mice. *J. Controlled Release 114*, 381−388.
(26) Marinelli, L., Gottschalk, K.-E., Meyer, A., Novellino, E., and Kessler, H. (2004) Human integrin $\alpha_v\beta_5$: homology modeling and ligand binding. *J. Med. Chem. 47*, 4166−4177.
(27) Bretscher, M. S. (1996) Moving membrane up to the front of migrating cells. *Cell 85*, 465−467.
(28) Marnie, R., Simon, B., Alison, W., Peter, S., and Jim, N. (2001) PDGF-regulated rab4-dependent recycling of $\alpha_v\beta_3$ integrin from early endosomes is necessary for cell adhesion and spreading. *Curr. Biol. 11*, 1392−1402.
(29) Suh, J., Wirtz, D., and Hanes, J. (2003) Efficient active transport of gene nanocarriers to the cell nucleus. *Proc. Natl. Acad. Sci. U.S.A. 100*, 3878−3882.
(30) Kulkami, R. P., Wu, D. D., Davis, M. E., and Fraser, S. E. (2005) Quantitating intracellular transport of polyplexes by spatio-temporal image correlation spectroscopy. *Proc. Natl. Acad. Sci. U.S.A. 102*, 7523−7528.
(31) Rejmna, J., Bragonzi, A., and Conese, M. (2005) Role of clathrin- and caveolae-mediated endocytosis in gene transfer mediated by lipo- and polyplexes. *Mol. Ther. 12*, 468−474.
(32) Gersdorff, K., Sanders, N. N., Vandenbroucke, R., Smedt, S. C., Wagner, E., and Ogris, M. (2006) The internalization route resulting in successful gene expression depends on both cell line and polyethylenimine polyplex type. *Mol. Ther. 14*, 745−753.

BC0700133

Available online at www.sciencedirect.com
ScienceDirect
Journal of Controlled Release 121 (2007) 146–155
journal of controlled release
www.elsevier.com/locate/jconrel

Optimization of (1,2-diamino-cyclohexane)platinum(II)-loaded polymeric micelles directed to improved tumor targeting and enhanced antitumor activity

Horacio Cabral [a], Nobuhiro Nishiyama [b], Kazunori Kataoka [a,b,c,*]

[a] *Department of Materials Engineering, Graduate School of Engineering, The University of Tokyo, 7-3-1 Hongo, Bunkyo-ku, Tokyo 113-8656, Japan*
[b] *Center for Disease Biology and Integrative Medicine, Graduate School of Medicine, The University of Tokyo, 7-3-1 Hongo, Bunkyo-ku, Tokyo 113-0033, Japan*
[c] *Center for NanoBio Integration, The University of Tokyo, 7-3-1 Hongo, Bunkyo-ku, Tokyo, 113-8656, Japan*

Received 19 March 2007; accepted 21 May 2007
Available online 29 May 2007

Abstract

Polymeric micelles are promising nanocarriers, which might enhance the efficacy of antitumor drugs. Herein, polymeric micelles incorporating dichloro(1,2-diamino-cyclohexane)platinum(II) (DACHPt), the oxaliplatin parent complex, were prepared through the polymer-metal complex formation of DACHPt with poly(ethylene glycol)-*b*-poly(glutamic acid) [PEG-*b*-P(Glu)] block copolymer having different lengths of the poly (glutamic acid) block [p(Glu): 20, 40, and 70 U]. The resulting micelles were studied with the aim of optimizing the system's biological performance. DACHPt-loaded micelles (DACHPt/m) were approximately 40 nm in diameter and had a narrow size distribution. *In vivo* biodistribution and antitumor activity experiments (CDF_1 mice bearing the murine colon adenocarcinoma C-26 inoculated subcutaneously) showed 20-fold greater accumulation of DACHPt/m at the tumor site than free oxaliplatin to achieve substantially higher antitumor efficacy. Moreover, the micelles prepared from PEG-*b*-P(Glu) with 20 U of P(Glu) exhibited the lowest non-specific accumulation in the liver and spleen to critically reduce non-specific accumulation, resulting in higher specificity to solid tumors. The antitumor effect of DACHPt/m was also evaluated on multiple metastases generated from intraperitoneally injected bioluminescent HeLa (HeLa-Luc) cells. The *in vivo* bioluminescent data indicated that DACHPt/m decreased the signal 10-to 50-fold compared to the control indicating a very strong antitumor activity. These results suggest that DACHPt/m could be an outstanding drug delivery system for oxaliplatin in the treatment of solid tumors.

Keywords: Polymeric micelles; DACHPt; Oxaliplatin; Biodistribution; Antitumor activity

1. Introduction

Oxaliplatin, oxalato(trans-*l*-1,2-diaminocyclohexane)platinum(II), is a third-generation platinum drug approved by the United States Food and Drug Administration in 2004 for the first-line treatment of advanced colorectal cancer in combination with 5-fluorouracil/folinic acid (5-FU/LV) [1]. The incorporation of oxaliplatin into the colorectal cancer program represents a major improvement in the treatment of the disease. The synergistic effects between oxaliplatin and 5-FU/LV significantly increased the response rates, improved the time-sensitive response parameters, and contributed to the removal of heretofore unresectable hepatic metastases, thereby changing the natural history of the malignancy. Nevertheless, oxaliplatin distributes rapidly to the whole body and, even though it shows better tolerability relative to other platinum drugs, cumulative peripheral distal neurotoxicity and acute dysesthesias restrain the range of working doses [2,3]. Consequently, enormous effort has been dedicated to develop drug delivery systems that increase the blood residence time of oxaliplatin and other platinum drugs, and target those drugs to solid tumors by taking advantage of the enhanced permeability and retention (EPR) effect [4]. Liposomes and macromolecular carriers (water soluble polymer–drug conjugates) have been the first attempts

* Corresponding author. Department of Materials Engineering, Graduate School of Engineering, The University of Tokyo, 7-3-1 Hongo, Bunkyo-ku, Tokyo 113-8656, Japan. Tel.: +81 3 5841 7138; fax: +81 3 5841 7139.
E-mail address: kataoka@bmw.t.u-tokyo.ac.jp (K. Kataoka).

0168-3659/$ - see front matter © 2007 Elsevier B.V. All rights reserved.
doi:10.1016/j.jconrel.2007.05.024

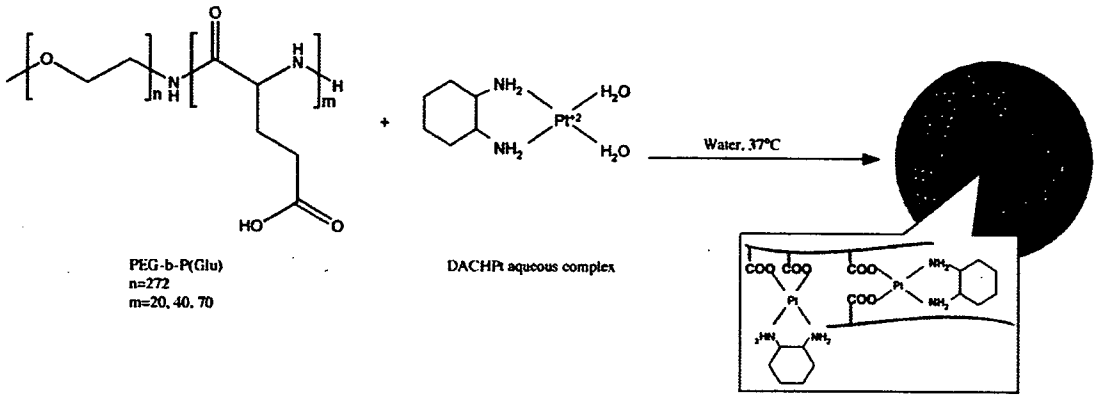

Fig. 1. Formation of DACHPt-loaded micelle (DACHPt/m).

to be considered [5–11]. However, successful formulations have not been developed yet due to unfavorable properties of platinum drugs. For example, the low water solubility of platinum drugs limits their loading efficacy into liposomal formulations (only 1 to 7% of drug loading). Moreover, liposomes incorporating the drug in the lipid bilayer showed rapid leakage of the drugs during storage and in the bloodstream [6]. In the case of macromolecular-drug formulations at high substitution ratios, they show reduced solubility due to the enlarged cohesive forces and to the cross-linking formation between polymer chains [8].

A novel approach to the design of nanocarriers for platinum drugs has been utilizing polymeric micelles [12–15]. Polymeric micelles present unique advantages over other types of drug-carrier systems: (i) prolonged blood circulation due to the efficient stealthy behavior of the dense shell of poly(ethylene glycol) (PEG), which hinders the adsorption of plasma proteins on the surface of the nanostructure and avoids recognition by the reticuloendothelial system (RES); (ii) easiness in encapsulating different compounds by modulating the micelle-forming block copolymers; (iii) reduced cumulative toxicity because of the micellar self-dissociation into unimers with molecular weight lower than that of the threshold of glomerular excretion; (iv) simplicity in size control by changing the chemical composition of block copolymers; (v) deeper tumor penetration due to the sub-100 nm size; (vi) facile management of the drug release in a controlled and environment-sensitive manner by modification of the drug-polymer system; and (vii) improved targeting capability by conjugating pilot molecules on the surface of micelles.

The first generation of platinum-drug-loaded micelles was prepared by the metal-complex formation between cis-dichlorodiammineplatinum(II) (cisplatin, CDDP) and poly(ethylene glycol)-*b*-poly(amino acid) block copolymers [16–21]. The exceptional physicochemical and biological properties of the CDDP-loaded micelle indicate them as an outstanding delivery system for CDDP complexes and a phase I clinical trial is being performed in United Kingdom (NC-6004, Nanocarrier, Japan). More recently, new platinum-drug-loaded polymeric micelles incorporating the oxaliplatin active complex were prepared by the complexation of dichloro(1,2-diaminocyclohexane)platinum(II) (DACHPt) with PEG-*b*-P(Glu) [22]. Previous studies demonstrated that the DACHPt-loaded micelle (DACHPt/m) might maintain its micellar structure for approximately 10 days in 10 mM PBS plus 150 mM NaCl, considerably longer than the stability of the CDDP-loaded micelles (ca 50 h) under the same conditions, while the drug was released from the micelle core in a sustained manner. Moreover, DACHPt/m showed remarkably prolonged blood circulation and more than 20-fold greater accumulation in tumor tissue compared to free oxaliplatin. According to these results, DACHPt/m seems to be an exceptionally promising carrier for the active complexes of oxaliplatin.

Herein, the *in vitro* and *in vivo* biological properties of DACHPt/m prepared with poly(ethylene glycol)-*b*-poly(glutamic acid) [PEG-*b*-P(Glu)] were studied with the aim of optimizing the biological performance of the micelle. Thus, PEG-*b*-P(Glu) having different P(Glu) block lengths (20, 40, and 70 U) were synthesized and used for the micelle preparation. DACHPt/m was phisicochemically characterized to determine the size, size distribution, zeta-potential, drug loading, and weight fraction of block copolymer. The *in vivo* behavior of DACHPt/m was assessed by the biodistribution and antitumor activity experiments using CDF_1 mice bearing the murine colon adenocarcinoma 26 (C-26). Although oxaliplatin had shown low efficacy against this tumor model [23], we found that DACHPt/m considerably increased the antitumor activity of the drug, probably by maintaining high drug levels within the tumor for a prolonged period. Furthermore, since chemotherapy is used in patients with metastatic disease and all the established therapies reveal poor efficiency at the late stage of the disease [24], new therapeutic strategies are urgently needed. Moreover, given that the very low prognosis of late-stage cervical carcinoma [25] (5 years after treatment 15% or fewer of women with stage IV cancer survive) is mainly due to metastasis to the abdomen or the lungs, the antitumor activity of DACHPt/m was evaluated against a bioluminescent intraperitoneal metastatic tumor model of cervical cancer.

2. Experimental

2.1. Materials

γ-benzyl L-glutamate was purchased from Sigma Chemical (St. Louis, MO). Bis(trichloromethyl)carbonate (triphosgene) was purchased from Tokyo Kasei Kogyo (Tokyo, Japan). *N,N-*

Table 1
DACHPt-loaded micelles (DACHPt/m) size, zeta-potential and drug loading

Micelle formulation	Size(nm)	Zeta-potential(mV)	Drug loading, [DACHPt]/[Glu]
DACHPt/m 12–20	37	−3	0.317
DACHPt/m 12–40	40	−4	0.323
DACHPt/m 12–70	41	−4	0.288

dimethylformamide (DMF) and 3-(4,5-dimethylthiazol-2-yl)-2,5-diphenyltetrazolium bromide (MTT) were obtained from Wako Pure Chemical (Osaka, Japan). Dichloro(1,2-diamminocyclohexane)platinum(II) (DACHPt) and $AgNO_3$ were purchased from Aldrich Chemical (Milwaukee, WI). α-methoxy-ω-aminopoly(ethylene glycol) (CH_3O–PEG–NH_2; Mw= 12,000) was purchased from Nippon Oil and Fats (Tokyo, Japan).

2.2. Cell lines and animals

Murine colon adenocarcinoma 26 (C-26) cells were kindly supplied by the National Cancer Center (Tokyo, Japan). C-26 cells were maintained in RPMI 1640 medium (Sigma Chemical) containing 10% fetal bovine serum in a humidified atmosphere containing 5% CO_2 at 37 °C. Bioluminescent HeLa (HeLa-Luc) cells were purchased from Xenogen (Alameda, CA). Luciferase stable-HeLa-Luc cells were maintained in Dulbecco's Modified Eagle Medium (Sigma Chemical Co., Inc.) containing 10% fetal bovine serum in a humidified atmosphere containing 5% CO_2 at 37 °C for no more than two weeks to assure luciferase luminescence stability.

Table 2
Accumulation ratios and area under the curve (AUC) ratios between tumor and normal organs at 48 h after administration of DACHPt-loaded micelles (DACHPt/m)[a] prepared with PEG-*b*-P(Glu) 12–40 and free oxaliplatin

Drug	Accumulation ratio				AUC ratio[b]	
	Tumor/ liver	Tumor/ spleen	Tumor/ kidney	Tumor/ liver	Tumor/ spleen	Tumor/ kidney
DACHPt/m 12–40	1.25	1.26	3.9	1.25	1.53	3.12
Oxaliplatin	0.9	0.18	0.42	1.1	0.32	0.9

[a] Dose: 0.1 mg per mouse on Pt basis.
[b] AUC calculated by trapezoidal rule up to 48 h.

Severe Combined Immunodeficiency (SCID) and CDF_1 mice (female; 18–20 g body weight; 6 weeks old) were purchased from Charles River Japan (Kanagawa, Japan). All animal experiments were carried out in accordance with the Guide for the Care and Use of Laboratory Animals as stated by the NIH. Sterile procedures were followed to assure that SCID mice were disease-free.

2.3. Preparation of PEG-b-P(Glu)

PEG-*b*-P(Glu) block copolymers were synthesized in accordance with the previously described synthetic method

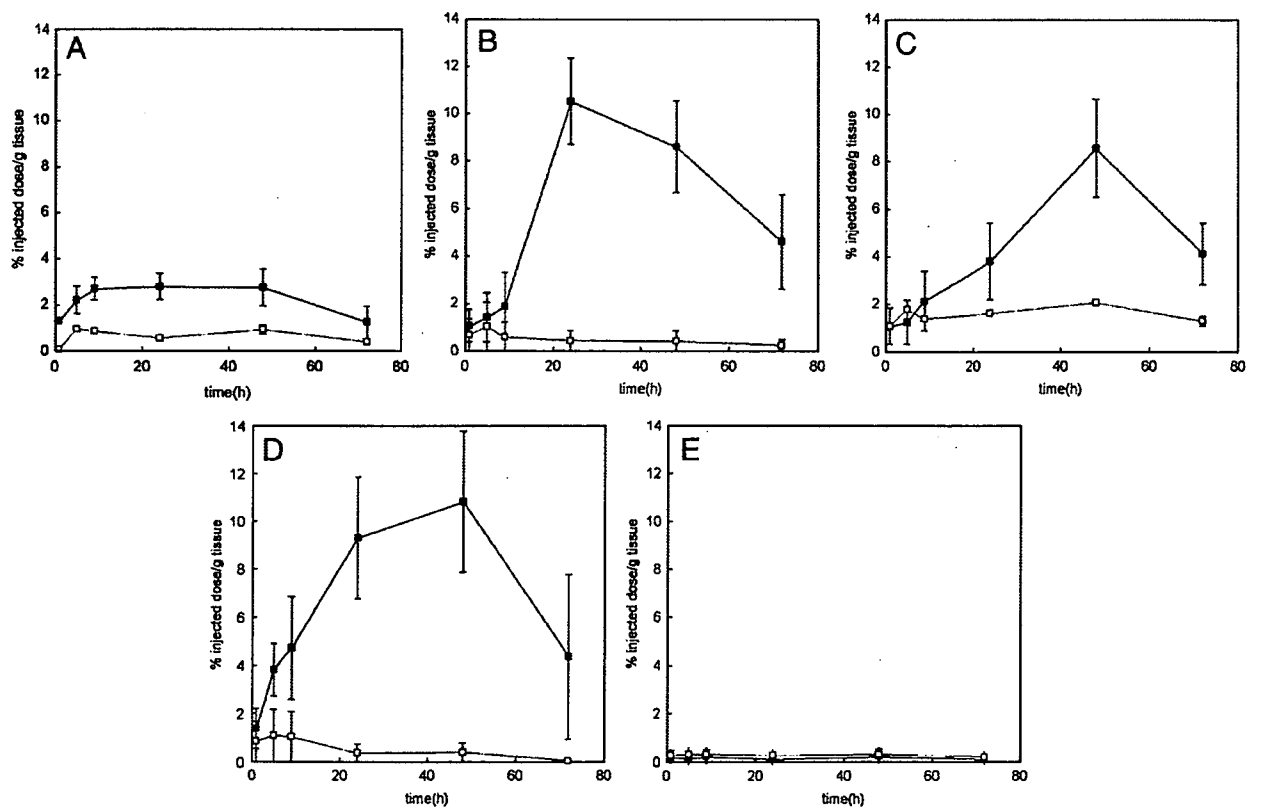

Fig. 2. Biodistribution of oxaliplatin (□) and DACHPt-loaded micelle (DACHPt/m) prepared with PEG-*b*-P(Glu) 12–40 (■): A. Kidney; B. Liver; C. Spleen; D. Tumor; E. Muscle. Data are expressed as averages±S.D.

[20] with a minor modification. Briefly, the *N*-carboxy anhydride of γ-benzyl L-glutamate was synthesized by the Fuchs–Farthing method using triphosgene. Then, *N*-carboxy anhydride of γ-benzyl L-glutamate was polymerized in DMF, initiated by the primary amino group of CH_3O–PEG–NH_2, to obtain PEG-*b*-poly(γ-benzyl L-glutamate) (PEG-*b*-PBLG) block copolymer with different PBLG block lengths (20, 40, and 70 U). The molecular weight distribution of PEG-*b*-PBLG was determined by gel permeation chromatography [column: TSK-gel $G3000_{HHR}$, $G4000_{HHR}$ (Tosoh, Yamaguchi, Japan); eluent: DMF containing 10 mM LiCl; flow rate: 0.8 ml/min; detector: refractive index (RI); temperature: 25 °C]. The polymerization degree of PBLG was verified by comparing the proton ratios of methylene units in PEG (–OCH_2CH_2–: δ=3.7 ppm) and phenyl groups of PBLG (–$CH_2C_6H_5$: δ=7.3 ppm) in ^{1}H-NMR measurement [JEOL EX270 (JEOL, Tokyo, Japan); solvent: DMSO-d_6; temperature: 80 °C]. PEG-*b*-PBLG was deprotected by mixing with 0.5 N NaOH at room temperature to obtain PEG-*b*-P(Glu). Complete deprotection was confirmed by ^{1}H-NMR measurement (solvent: D_2O; temperature: 25 °C). The compositions of PEG-*b*-P(Glu) are abbreviated as PEG-*b*-P(Glu) 12–20, PEG-*b*-P(Glu) 12–40 and PEG-*b*-P(Glu) 12–70 for the different P(Glu) block lengths (20, 40, and 70 U, respectively).

2.4. Preparation of DACHPt-loaded micelles (DACHPt/m)

DACHPt/m were prepared according to a previously described method [22]. Briefly, DACHPt (5 mM) was suspended in distilled water and mixed with silver nitrate ([$AgNO_3$]/[DACHPt]=1) to form an aqueous complex. The solution was kept in the dark at 25 °C for 24 h. AgCl precipitates found after the reaction were eliminated by centrifugation. Afterward, the supernatant was purified by passage through a 0.22 μm filter. Then, PEG-*b*-P(Glu) 12–20, 12–40, or 12–70 ([Glu]=5 mmol/liter) was added to DACHPt aqueous complex solution ([DACHPt]/[Glu]=1.0) and reacted for 120 h to prepare DACHPt/m. The prepared micelles were purified by ultrafiltration [molecular weight cutoff size (MWCO): 100,000]. The size distribution of DACHPt/m was evaluated by the dynamic light scattering (DLS) measurement at 25 °C using a Photal DLS-7000 dynamic laser scattering spectrometer (Otsuka Electronics, Osaka, Japan). The zeta-potential of DACHPt/m was determined using a Zetasizer Nano ZS90 (Malvern Instruments, Worcestershire, United Kingdom). The Pt content of the micelles was determined by an ion coupled plasma-mass spectrometer (4500 ICP-MS; Hewlett Packard, Palo Alto, CA).

2.5. Biodistribution

In order to analyze the fate of oxaliplatin and DACHPt/m *in vivo*, CDF_1 mice (female, n=6) were injected subcutaneously with C-26 cells (1×10^6 cells/ml). Fourteen days later, oxaliplatin or DACHPt/m prepared with PEG-*b*-P(Glu) 12–40 were intravenously injected by the tail vein at a dose of 100 μg/mouse on a platinum basis. Mice were sacrificed after defined time periods (1, 4, 8, 24, 48, and 72 h).

To assess the effect of formulation on the tissue distribution, CDF_1 mice (female, n=6) bearing s.c. C-26 tumors were intravenously administered oxaliplatin or DACHPt/m prepared with PEG-*b*-P(Glu) with different P(Glu) lengths (20, 40, and

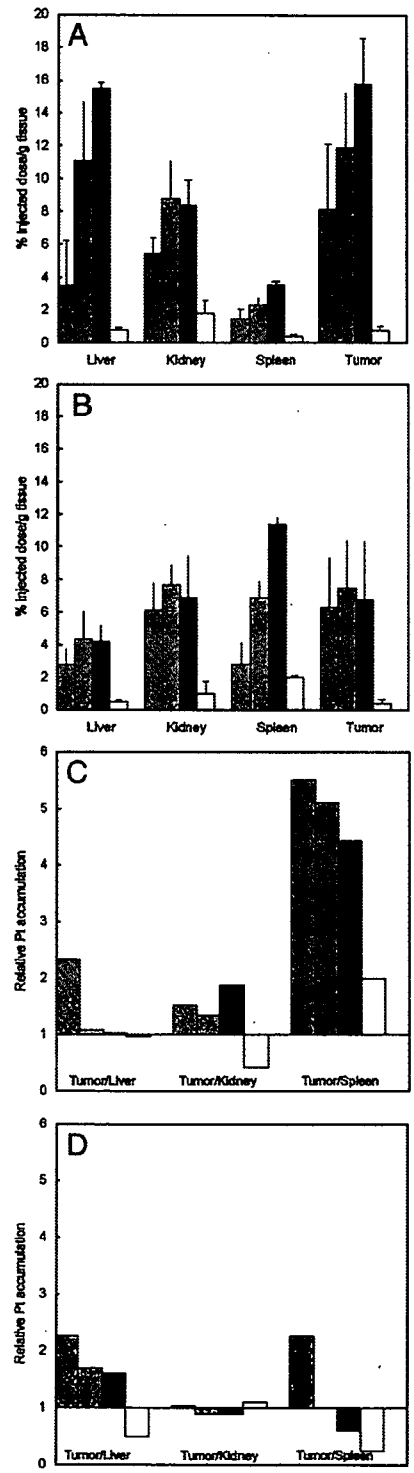

Fig. 3. Biodistribution of DACHPt-loaded micelle (DACHPt/m) prepared with PEG-*b*-P(Glu) 12–20(▨), PEG-*b*-P(Glu) 12–40(▨), PEG-*b*-P(Glu) 12–70(■) and oxaliplatin (□): A. 24 h; B.48 h; C. 24 h tumor/organ ratio; D. 48 h tumor/organ ratio. Data are expressed as averages±S.D.

70 U) at 100 μg/mouse on a platinum basis. Mice were sacrificed at 24 and 48 h post-incubation.

Tumor, liver, kidney, spleen, and muscle were collected. Blood was collected from the inferior vena cava, heparinized and centrifuged to obtain the plasma. Tissue samples were washed in ice-cold saline and weighed after removing excess fluid. All samples were dissolved in HNO_3 and evaporated to dryness. The Pt concentration was measured by ICP-MS after the samples were redissolved in 5 N HCl. The area under the curve (AUC) was calculated by the trapezoidal rule.

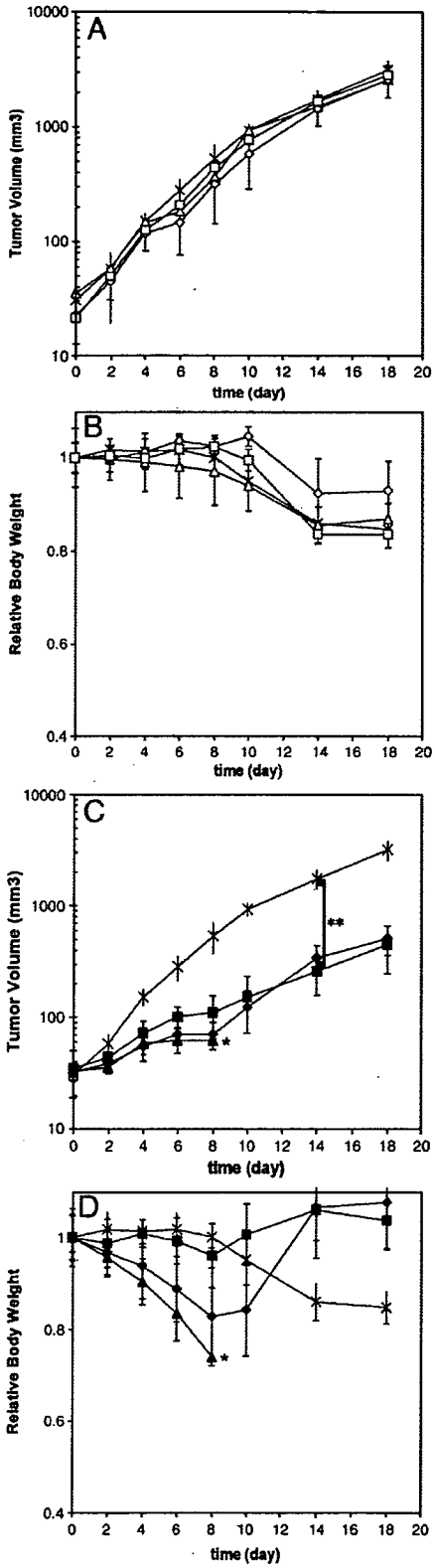

Fig. 4. Antitumor activity of DACHPt-loaded micelle (DACHPt/m) prepared with PEG-*b*-P(Glu) 12–40 against s.c. C-26 tumor model (n=5). Saline(×); oxaliplatin at 6 mg/kg(△); 4 mg/kg(◇); 2 mg/kg(□). DACHPt-loaded micelle (DACHPt/m) 12–40 at 6 mg/kg(▲); 4 mg/kg(◆); 2 mg/kg(■). A. Tumor volume (mm^3) for oxaliplatin treatment; B. Relative body weight of mice for oxaliplatin treatment; C. Tumor volume (mm^3) for DACHPt/m treatment; D. Relative body weight of mice for DACHPt/m treatment. Data are expressed as averages±S.D. *Toxic death. **$p<0.001$.

2.6. Antitumor activity assay

CDF_1 mice (female, n=6) were inoculated subcutaneously with C-26 cells (1×10^6 cells/ml). Tumors were allowed to grow for 1 week (the size of tumor at this point was approximately 30 mm^3 or 100 mm^3). Subsequently, mice were treated i.v. 4 times at 2-day intervals at doses of 2, 4, 6 and 10 mg/kg of oxaliplatin or 2, 4 and 6 mg/kg (on a platinum base) of DACHPt/m prepared with PEG-*b*-P(Glu) 12–20 or PEG-*b*-P (Glu) 12–40. The antitumor activity was evaluated in terms of tumor size (V), as estimated by the following equation:

$$V = a \times b^2/2$$

where a and b are the major and minor axes of the tumor measured by a caliper, respectively. The body weight was measured simultaneously and was taken as a parameter of systemic toxicity. The statistical analysis of animal data was carried out by the unpaired t-test.

2.7. Antitumor activity in a bioluminescent intraperitoneal metastasis model

SCID mice (female, n=5) were inoculated intraperitoneally with Hela-Luc cells (5×10^5 cells/ml). Tumors were allowed to grow for 3 days. Subsequently, mice were treated i.v. 3 times at 2-day intervals at doses of 4 and 6 mg/kg (on a platinum base) of oxaliplatin or DACHPt/m prepared with PEG-b-P(Glu) 12–20. *In vivo* bioluminescent imaging (BLI) was performed with an IVIS Imaging System (Xenogen) comprised of a highly sensitive, cooled CCD camera mounted in a light-tight specimen box. Images and measurements of bioluminescent signals were acquired and analyzed using Living Image software (Xenogen). Ten minutes prior to *in vivo* imaging, animals received the substrate D-luciferin (Biosynth) at 150 mg/kg in PBS by intraperitoneal injection and were anesthetized using 1–3% isoflurane (Abbott Laboratories, North Chicago, IL). Animals were placed onto a warmed stage inside the camera box and received continuous exposure to 1–2% isoflurane to sustain sedation during imaging. Imaging times ranged from 10 to 60 s, depending on the bioluminescence of the metastatic lesions. Five mice were imaged at a time. Tumor growth was monitored

by BLI every second day for 18 days. The light emitted from the bioluminescent tumors was detected *in vivo* by the IVIS Imaging System, was digitized and electronically displayed as a pseudocolor overlay onto a gray scale animal image. Regions of interest (ROI) from displayed images were drawn around the tumor sites and quantified as photons/second using the Living Image software. The statistical analysis of animal data was carried out by the unpaired *t*-test.

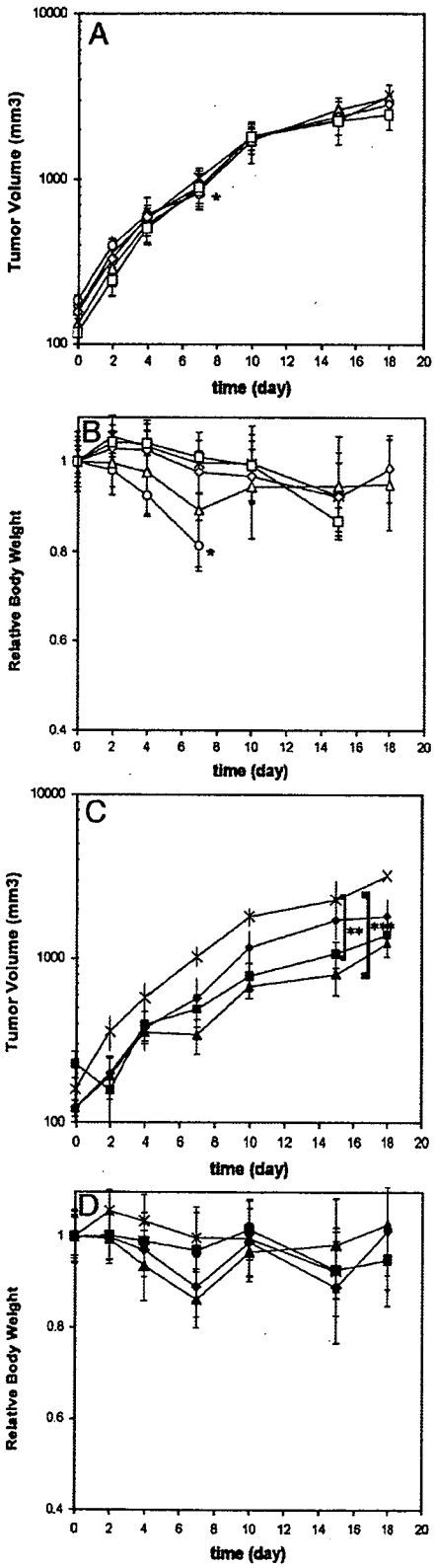

Fig. 5. Antitumor activity of DACHPt-loaded micelle (DACHPt/m) prepared with PEG-*b*-P(Glu) 12–20 against s.c. C-26 tumor model ($n=6$). Saline(×); oxaliplatin at 10 mg/kg(○); 6 mg/kg(△); 4 mg/kg(◇); 2 mg/kg(□). DACHPt-loaded micelle (DACHPt/m) 12–20 at 6 mg/kg(▲); 4 mg/kg(◆); 2 mg/kg(■). A. Tumor volume (mm^3) for oxaliplatin treatment; B. Relative body weight of mice for oxaliplatin treatment; C. Tumor volume (mm^3) for DACHPt/m treatment; D. Relative body weight of mice for DACHPt/m treatment. Data are expressed as averages±S.D. *Toxic death. $^{**}p<0.01$. $^{***}p<0.005$.

3. Results

3.1. Micelle characterization

The metal-polymer complex formation between DACHPt and the carboxylic group of the p(Glu) in the PEG-*b*-P(Glu) led to the formation of narrowly distributed micellar assemblies (Fig. 1) with average diameters of approximately 40 nm (Table 1). The increase in the length of the p(Glu) block slightly enlarged the diameter of DACHPt/m (Table 1). The drug content in the micelles was determined to be remarkably high in all the micelle formulations (Table 1). The [DACHPt]/[Glu] molar ratios in DACHPt/m were found to be similar for all the formulations.

3.2. Biodistribution

3.2.1. Biodistribution of free oxaliplatin and DACHPt/m prepared with PEG-b-P(Glu) 12–40

The biodistribution study was performed on CDF_1 mice ($n=6$) bearing s.c. C-26 tumors. Oxaliplatin or DACHPt/m prepared with PEG-*b*-P(Glu) 12–40 were i.v. injected. In previous studies, DACHPt/m prepared with PEG-*b*-P(Glu) 12–40 have shown remarkably prolonged blood circulation, whereas free oxaliplatin was promptly removed from circulation. The Pt in plasma was determined to be 15% of the injected dose at 24 h post-injection, and more than 8% even at 48 h after injection for DACHPt/m [22]. This prolonged blood circulation of DACHPt/m was reasonably associated with the high kinetic stability of the micelles in phosphate buffered saline at 37 °C [22].

The accumulations of oxaliplatin and DACHPt/m in normal tissues (kidney, liver, spleen, and muscle) and solid tumor (C-26 cells) are shown in Fig. 2. Oxaliplatin was rapidly distributed to each organ in agreement with its rapid plasma clearance. In contrast, DACHPt/m showed cumulative accumulation in each organ and solid tumor ($p<0.001$) due to its remarkably prolonged blood circulation time, and the Pt level in the liver, spleen, and tumor continuously increased up to approximately 48 h after injection (Fig. 2). Consequently, the DACHPt/m exhibited 20-, 4-, and 25-fold higher accumulation in the liver, spleen, and tumor, respectively, than oxaliplatin at 48 h after injection. To assess the selectivity to the solid tumor, the

accumulation ratios and area under the Pt concentration-time curve (AUC) ratios of the tumor to normal tissues at 48 h after injection are summarized in Table 2. The area under the Pt concentration-time curve was calculated based on the trapezoidal rule up to 48 h. As shown in Table 2, the tumor to kidney, liver and spleen ratios were lower than 1 for oxaliplatin, suggesting no selectivity to the tumor. In contrast, the DACHPt/m exhibited accumulation and AUC ratios higher than 1.0, suggesting its selective accumulation in the tumor.

3.2.2. *Effect of P(Glu) block length on the biodistribution of micelles*

The biodistribution of the micelles prepared from PEG-*b*-P(Glu) with different p(Glu) block units in tumor-bearing mice was examined and is shown in Fig. 3. The Pt accumulation levels were studied at 24 and 48 h. All the DACHPt/m formulations showed elevated Pt levels at the tumor (Fig. 3A and B). Importantly, the amount of Pt in liver was directly correlated with the length of the p(Glu) block forming DACHPt/m. The tumor targeting efficiency of the micelles was estimated by calculating the ratio of the accumulated dose in the tumor site against the accumulated dose in the organs (Fig. 3C and D). From these results, DACHPt delivery to the tumor site by a micellar carrier seems to be extremely efficient, since all the micelles showed higher tumor/organ accumulation ratios. This efficiency was maximized for the PEG-*b*-P(Glu) 12–20-micelle formulation showing the lowest non-specific accumulation in normal tissues, thus achieving the highest relative tumor targeting. Such enhanced tumor targeting will permit expanding the therapeutic window of the micelle.

3.3. *Antitumor activity*

To evaluate the antitumor activity of DACHPt/m, CDF1 mice ($n=6$) bearing subcutaneous C-26 cells were treated i.v. four times at 2-day intervals with oxaliplatin at doses of 2, 4, 6, and 10 mg/kg or DACHPt/m (prepared with PEG-*b*-P(Glu) 12–40 and 12–20) at doses of 2, 4, and 6 mg/kg on a Pt basis. Each drug was intravenously injected on days 7, 9, 11, and 13 after inoculation, and the tumor volume after the treatment by oxaliplatin or DACHPt/m with PEG-*b*-P(Glu) 12–40 and 12–20 is shown in Figs. 4 and 5 (A and C), respectively. The relative body weight after the treatment was also monitored and shown in Figs. 4 and 5 (B and D).

The mice treated with 10 mg/kg of oxaliplatin showed toxic death after the fourth injection. Although animals treated with lower oxaliplatin doses did not show significant body weight loss, no inhibition of the tumor growth rate was observed ($p>0.05$). In contrast, the mice treated with 2 mg/kg of DACHPt/m prepared with PEG-*b*-P(Glu) 12–40 achieved significant reduction in the tumor growth rate ($p<0.001$ at day 14) without showing any body weight loss (Fig. 4C and D). Even higher tumor growth inhibition was observed for the mice treated with 4 mg/kg of PEG-*b*-P(Glu) 12–40 DACHPt/m

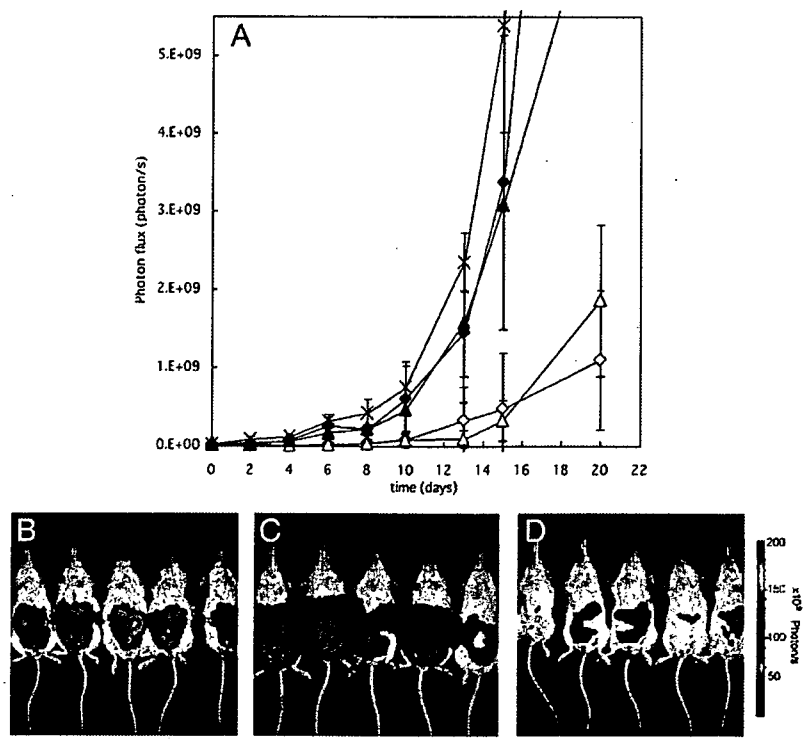

Fig. 6. Antitumor activity of DACHPt-loaded micelle (DACHPt/m) prepared with PEG-*b*-P(Glu) 12–20 against i.p. HeLa-Luc metastases ($n=5$). A. Relative photon flux from intraperitoneal metastatic sites of HeLa-luc *in vivo* treated with oxaliplatin or DACHPt-loaded micelle (DACHPt/m): Saline(×); oxaliplatin at 6 mg/kg(▲); 4 mg/kg(◆); DACHPt/m 12–20 at 6 mg/kg(△); 4 mg/kg(◇). Data are expressed as averages±S.D. *In vivo* bioluminescent images from HeLa-Luc i.p metastases at day 15: B. Saline; C. oxaliplatin 6 mg/kg; D. DACHPt/m 12–20 at 6 mg/kg.

($p<0.001$ at day 14); however, the 20% body weight loss after fourth injection suggests toxicity intensification. Increasing the DACHPt/m dose to 6 mg/kg resulted in 4 toxic deaths at day 8. The PEG-*b*-P(Glu) 12–20 micelle formulation reduced the toxicity while retaining the antitumor activity of the micelle (Fig. 5C and D). At 2 mg/kg or 4 mg/kg, this micelle formulation showed improved antitumor effect ($p<0.05$ at day 15 for 2 mg/kg; $p<0.01$ at day 15 for 4 mg/kg) compared with oxaliplatin without showing any body weight loss. At 6 mg/kg, the best tumor growth rate reduction was achieved ($p<0.005$ at day 15). The highest dose of this formulation in this experiment did not reach the lethal dose. Thus, PEG-*b*-P(Glu) 12–20 formulation for DACHPt/m seems to radically reduce drug toxicity with maintaining its potent antitumor effect, thus enlarging the therapeutic window. In addition, toxic death with DACHPt/m appeared at lower drug equivalent concentration than with oxaliplatin mainly due to the extremely high plasma AUC of DACHPt/m [22], but also because oxaliplatin is a prodrug of DACHPt. Thus, even though the drug equivalent of DACHPt/m to induce toxic death should be compared with DACHPt, it is very difficult to administer DACHPt alone due to its poor solubility.

Since DACHPt/m prepared with PEG-P(Glu) 12–70 showed higher accumulation to the liver and spleen than DACHPt/m prepared from PEG-P(Glu) 12–20 and 12–40, it will probably not increase the efficiency of the carrier. Therefore, its antitumor activity was not tested.

3.4. Antitumor activity in a bioluminescent intraperitoneal metastasis model

To evaluate the *in vivo* antitumor effect of DACHPt/m on multiple metastases generated from i.p inoculated Hela-Luc cells, SCID mice ($n=5$) were treated with free oxaliplatin or DACHPt/m beginning on day 4 post-injection. Mice with images indicating a successful i.p. inoculation on day 0 and showing *in vivo* evidence of metastasis by day 4 were placed in the drug treatment group. Free oxaliplatin or DACHPt/m were administered i.v a total of three times on day 0, 2, and 4. To quantify the bioluminescent data from metastasis, the photons emitted from the ROI in the whole animal (ventral images) were measured. The mean total photons/s were calculated from all mice. The *in vivo* bioluminescent data indicated that there was a 10-to 50-fold drop in the signal after DACHPt/m treatment (Fig. 6A). Images taken on day 15 (Fig. 6B, C, and D) indicated that DACHPt/m reduced tumor spreading in the peritoneal cavity, showing their strong growth inhibitory effect against the metastatic tumors.

4. Discussion

DACHPt/m were designed to have an extended blood circulation and a selective and high accumulation at the tumor site by the EPR effect. The average diameter of 40 nm and the hydrophilic PEG shell surrounding the micelle core are determinant features of DACHPt/m to avoid the uptake by the RES. Moreover, the sub-100 nm size of micellar nanocarriers might be optimal to achieve a remarkably high tumor extravasation efficiency and deep tumor penetration regardless of the tumor type [26]. The pharmacokinetic parameters of polymeric micelles are significantly modulated by the copolymer architecture. In this regard, the length of the micelle core-forming block not only determines the drug loading capacity of the micelle but also contributes largely to the physicochemical properties of the micelles, whereas PEG length and PEG surface density of micelles have been strongly associated with their long-circulating properties [27,28]. In this study, we prepared DACHPt/m using PEG-*b*-P(Glu) bearing different lengths of p (Glu) chain. We found that this variation considerably influences the biodistribution of micelles and thereby their antitumor activity as well as the final therapeutic window.

Drug dosage in chemotherapy is decided in part based on the competing goals of maximizing the death of malignant cells while minimizing damage to healthy cells. In the case of oxaliplatin, the major and most frequent dose-limiting toxicity observed in clinical trials was neurotoxicity [1]. Toxicological studies performed on rats with cisplatin and oxaliplatin demonstrated that the main target of neurotoxicity was the dorsal root ganglion (DRG) [29]. Although cisplatin accumulated in the DRG at a higher extent than oxaliplatin, the latter displayed more morphometric changes to the DRG after an 8-week recovery period, and this was correlated with a greater retention of oxaliplatin by the DRG in comparison with cisplatin. In contrast, neurotoxic studies revealed that CDDP-loaded micelles did not show any neurotoxicity or neuronal degeneration in rats [21]. This result might be attributed to the marked restriction of platinum accumulation into nervous tissue for the CDDP-loaded micelle, owing to the micelle size and its hydrophilic surface. Since CDDP-loaded micelles and DACHPt/m showed comparable prolonged blood circulation, preferential tumor targeting, and low accumulation in organs (Fig. 2) [20], similar reduction in the platinum accumulation at nervous tissue should be expected for DACHPt/m. Moreover, it has also been suggested that the oxalate group on oxaliplatin might immobilize calcium ions, thereby altering the amplitude of voltage-gated sodium channels of neurons [30]. The absence of an oxalate group in the DACHPt/m formulations eliminates this kind of neuronal damage.

The use of oxaliplatin is also associated with the development of severe sinusoidal injury, an aspect that had not been considered in the earlier clinical trials of oxaliplatin [31,32]. In this regard, the CDDP-loaded micelle prepared with PEG-*b*-P(Glu) 12–40 has shown transient hepatic dysfunction in rats directly related to accumulation of the micelle in liver [21]. In the present study, DACHPt/m prepared with PEG-*b*-P(Glu) 12–40 showed biphasic behavior in liver accumulation, and the Pt level in the liver remarkably increased after 8 h post-injection (Fig. 2B). Thus, the avoidance of liver uptake would be critical for the development of a clinically effective DACHPt/m formulation. We previously reported that the CDDP-loaded micelles also showed rapid accumulation of the micelle in the liver due to the morphological changes of the micelle accompanied by the release of CDDP during circulation [20]. However, such liver accumulation of the CDDP-loaded micelles was reduced for the micelle formulation from PEG-*b*-P(Glu) with a longer PEG segment [20]. Thus, the

coverage of the nanoparticles with PEG palisades is likely to be a crucial factor in the reduced liver accumulation. In this study, we evaluated the effects of the P(Glu) lengths of PEG-*b*-P(Glu) on the accumulation of the micelles in normal tissues and tumors. As a result, the micelles prepared with PEG-*b*-P(Glu) 12–20 showed considerably reduced accumulation in the liver (Fig. 3), resulting in critically reduced toxicity and, in particular, permitted a dosage increase (Fig. 5). Possibly, the use of PEG-*b*-P(Glu) with shorter P (Glu) segments may allow the formation of DACHPt/m with effective surface coverage by PEG probably due to reduced micellar core size, leading to reduction of the liver accumulation of the micelles.

DACHPt/m, prepared with PEG-b-P(Glu) 12–40 or 12–20, presented a remarkable, statistically relevant *in vivo* antitumor activity (Figs. 4 and 5), whereas free oxaliplatin failed to suppress tumor growth. The improved performance of DACHPt/m could be attributed to several aspects. The most distinguishable one is the high and preferential accumulation of DACHPt/m in the tumor due to the prolonged circulation of micelles in the bloodstream as well as the aforementioned EPR effect. In this study, DACHPt/m showed 10 times higher tumor accumulation than free oxaliplatin after 24-h post-injection, and such accumulation was maintained for an extended period (Figs. 2 and 3). On the other hand, free oxaliplatin was rapidly cleared from the bloodstream and the drug level at the tumor site was particularly low (Fig. 2). This accumulation level may be lower than the minimal amount needed to attain an efficient *in vivo* antitumor activity.

The avoidance of permanent drug inactivation by protein binding through the complexation of the platinum to the carboxylic groups in the micelle core could also be responsible for the improved biological performance of DACHPt/m over oxaliplatin. It was previously reported that, immediately after a 1 h infusion of oxaliplatin, approximately 5–30% of the drug is unbound, 10–30% is protein-bound, and 40% form complexes with hemoglobin and small molecular weight compounds in erythrocytes. Three hours later, no oxaliplatin is detectable in the plasma ultrafiltrate and only 10% is detectable in urine [33,34]. Furthermore, as many as 17 biotransformation products of oxaliplatin have been described (conjugation with methionine, cysteine, glutathione, and other low molecular weight species), but only the minor complexes $DACHPtCl_2$, $[DACHPt(H_2O)Cl]^+$ and $[DACHPt(H_2O)_2]^{2+}$ retain the ability to bind to DNA to exert the cytotoxic activity [35,36]. Among them, the dihydroxy product of oxaliplatin has been shown to have significantly greater cellular uptake and cytotoxic properties than its parent compound [37]. However, it represents a very small amount of the total plasma platinum pool after oxaliplatin administration, and therefore might not be a determinant for oxaliplatin cytotoxicity. Moreover, the formation process of $[DACHPt(H_2O)_2]^{2+}$ involves the formation of a reversible intermediate, oxalato monodentate compound, and the dissociation constant for the ring-opening step is below physiological pH (pKa=7.16). This implies that at physiological pH, the reaction favors the deprotonation of the open-ring form and the subsequent formation of the dihydroxy complex, whereas under the acidic conditions of solid tumors, ring-closure is favored and the rapid formation of oxaliplatin would be expected [38]. For DACHPt/m, the biotransformation products might be considerably different from those of oxaliplatin, and probably affect the *in vivo* performance of the drug. Since the discharge of DACHPt products from the micelle core occurs only after cleavage of the polymer-metal complex by chloride ions, and this release is enhanced at low pH, DACHPt/m probably set up conditions that favor the formation of active complexes of oxaliplatin, including the highly active $[DACHPt(H_2O)_2]^{2+}$, leading to an improved efficacy of the drug. Moreover, selective intracellular release of DACHPt complexes might occur after internalization of the micelles by endocytosis in cancer cells. As a result, DACHPt complexes may avoid extracellular inactivation and may readily induced intracellular damage.

Since systemic chemotherapy is not regarded as curative in patients with metastatic tumors and all the established therapies show low efficiency at the late stage of the disease, the antitumor activity of DACHPt/m against an i.p. metastatic tumor model was evaluated to test the potential use of micelles as a therapeutic strategy. Monitoring the development of metastatic disease is currently possible *in vivo* with the use of small animal imaging technologies including bioluminescent imaging. The results demonstrate that free oxaliplatin failed to suppress HeLa-Luc metastatic growth at any dose, whereas DACHPt/m showed a high antitumor activity while controlling tumor dissemination in the peritoneal cavity. This marked difference could be correlated to the extended blood circulation and preferential tumor accumulation of DACHPt/m, although further experiments are necessary to determine the effect of the metastatic disposition on the efficiency of the micelle. The present results revealed that DACHPt/m has a high level of antitumor activity not only on primary solid tumors but also against metastatic tumors, suggesting that DACHPt/m could be an outstanding drug delivery system for metastasis treatment.

In conclusion, we have demonstrated that decreasing the length of the core-forming block of DACHPt/m augmented their tumor specificity and drastically diminished their toxicity. Moreover, the high and preferential accumulation of the micelles at the tumor site resulted in considerable antitumor activity of DACHPt/m against primary and metastatic tumor models. Thus, DACHPt/m might be an exceptional drug delivery system for oxaliplatin active complexes.

Acknowledgments

This research was supported by a Grant-in-Aid for Scientific Research from Ministry of Education, Culture, Sports, Science and Technology of Japan as well as by the Project on the Materials Development for Innovative Nano-Drug Delivery Systems from the Ministry of Education, Culture, Sports, Science and Technology (MEXT), Japan.

References

[1] A. Ibrahim, S. Hirschfeld, M.H. Cohen, D.J. Griebel, G.A. Williams, R. Pazdur, FDA drug approval summaries: oxaliplatin, Oncologist 9 (2004) 8–12.

[2] J.M. Extra, M. Espie, F. Calvo, Phase I study of oxaliplatin in patients with advanced cancer, Cancer Chemother. Pharmacol. 25 (1990) 299–303.

[3] G. Mathé, Y. Kidani, M. Segiguchi, M. Eriguchi, G. Fredj, G. Peytavin, J.L. Misset, S. Brienza, F. de Vassals, E. Chenu, C. Bourut, Oxalato-platinum or l-OHP, a third generation platinum complex: an experimental and clinical appraisal and preliminary comparison with cis-platinum and carboplatinum, Biomed. Pharmacother. 43 (1989) 237–250.
[4] Y. Matsumura, H. Maeda, A new concept for macromolecular therapeutics in cancer chemotherapy: mechanism of tumoritropic accumulation of proteins and the antitumor agent SMANCS, Cancer Res. 46 (1986) 6387–6392.
[5] M. Yatvin, H. Miihlensiepen, W. Porschen, L. Feinendegen, J. Weinstein, Selective delivery of liposome-associated cis-dichloro-diammine platinum (II) by heat and its influence on tumor drug uptake and growth, Cancer Res. 41 (1981) 1602–1607.
[6] R. Perez-Soler, Liposomes as carriers of antitumor agents: toward a clinical reality, Cancer Treatment Rev. 16 (1989) 67–82.
[7] R. Perez-Soler, I. Han, S. Al-Baker, A.R. Khokhar, Lipophilic platinum complexes entrapped in liposomes: improved stability and preserved antitumor activity with complexes containing linear alkyl carboxylate leaving groups, Cancer Chemother. 33 (1994) 378–384.
[8] D. Avichechter, B. Schechter, R. Arnon, Functional polymers in drug delivery: carrier-supported CDDP (cis-platin) complexes carboxylates — effect on human ovarian carcinoma, React. Funct. Polym. 36 (1998) 59–69.
[9] B. Schechner, A. Newman, M. Wilnek, R. Arnon, Soluble polymers as carriers of cis-platinum, J. Control. Release 39 (1989) 75–87.
[10] X. Lin, Q. Zhang, J.R. Rice, D.R. Stewart, D.P. Nowotnik, S.B. Howell, Improved targeting of platinum chemotherapeutics. The antitumour activity of the HPMA copolymer platinum agent AP5280 in murine tumour models, Eur J Cancer. 40 (2004) 291–297.
[11] J.R. Rice, J.L. Gerberich, D. Nowotnik, S.B. Howell, Preclinical efficacy of AP5346, a novel diaminocyclohexane-platinum tumor-targeting drug delivery system, Clin. Cancer Res. 12 (2006) 2248–2254.
[12] K. Kataoka, G.S. Kwon, M. Yokoyama, Y. Sakurai, T. Okano, Block copolymer micelles as vehicles for drug delivery, J. Control. Release 24 (1993) 119–132.
[13] C. Allen, D. Mysinger, A. Eisenberg, Nano-engineering block copolymer aggregates for drug delivery, Colloids Surf., B Biointerfaces 16 (1999) 3–27.
[14] N. Nishiyama, K. Kataoka, Nano-structured devices based on block copolymer assemblies for drug delivery: designing structures for enhanced drug function, Adv. Polym. Sci. 193 (2006) 67–101.
[15] H.M. Aliabadi, A. Lavasanifar, Polymeric micelles for drug delivery, Expert Opin. Drug Deliv. 3 (2006) 139–161.
[16] N. Nishiyama, M. Yokoyama, T. Aoyagi, T. Okano, Y. Sakurai, K. Kataoka, Preparation and characterization of self-assembled polymer-metal complex micelle from cis-dichlorodiammineplatinum(II) and poly(ethylene glycol)-poly(a,b-aspartic acid) block copolymer in an aqueous medium, Langmuir 15 (1999) 377–383.
[17] N. Nishiyama, K. Kataoka, Preparation and characterization of size-controlled polymeric micelle containing cis-dichlorodiammineplatinum(II) in the core, J Control. Release 74 (2001) 83–94.
[18] N. Nishiyama, Y. Kato, Y. Sugiyama, K. Kataoka, Cisplatin-loaded polymer-metal complex micelle with time-modulated decaying property as a novel drug delivery system, Pharm. Res. 18 (2001) 1035–1041.
[19] N. Nishiyama, F. Koizumi, S. Okazaki, Y. Matsumura, K. Nishio, K. Kataoka, Differential gene expression profile between PC-14 cells treated with free cisplatin and cisplatin-incorporated polymeric micelles, Bioconjug. Chem. 14 (2003) 449–457.
[20] N. Nishiyama, S. Okazaki, H. Cabral, M. Miyamoto, Y. Kato, Y. Sugiyama, K. Nishio, Y. Matsumura, K. Kataoka, Novel cisplatin-incorporated polymeric micelles can eradicate solid tumors in mice, Cancer Res. 63 (2003) 8977–8983.
[21] H. Uchino, Y. Matsumura, T. Negishi, F. Koizumi, T. Hayashi, T. Honda, N. Nishiyama, K. Kataoka, S. Naito, T. Kakizoe, Cisplatin-incorporating polymeric micelles (NC-6004) can reduce nephrotoxicity and neurotoxicity of cisplatin in rats, Br. J. Cancer 93 (2005) 678–687.
[22] H. Cabral, N. Nishiyama, S. Okazaki, H. Koyama, K. Kataoka, Preparation and biological properties of dichloro(1,2-diaminocyclohexane)platinum (II) (DACHPt)-loaded polymeric micelles, J. Control. Release 101 (2005) 223–232.
[23] T. Tashiro, Y. Kawada, Y. Sakurai, Y. Kidani, Antitumor activity of a new platinum complex: oxalato (trans-l-diaminocyclohexane) platinum (II): new experimental data, Biomed. Pharmacother. 43 (1989) 251–260.
[24] S. Oppenheimer, Cellular basis of cancer metastasis: a review of fundamentals and new advances, Acta Histochem. 108 (2006) 327–334.
[25] Cervical cancer, NIH Consens. Statement 14 (1996) 1–38.
[26] A. Lukyanov, Z. Gao, L. Mazzola, V.P. Torchilin, Polyethylene glycol-dyacyllipid micelles demonstrate increased accumulation in subcutaneous tumors in mice, Pharm. Res. 19 (2002) 1424–1429.
[27] G.S. Kwon, S. Suwa, M. Yokoyama, T. Okano, Y. Sakurai, K. Kataoka, Enhanced tumor accumulation and prolonged circulation times of micelles-forming poly(ethyleneoxide-aspartate) block copolymers-adriamycin conjugates, J. Control. Release 29 (1994) 17–23.
[28] M. Yokoyama, T. Okano, Y. Sakurai, S. Fukushima, K. Okamoto, K. Kataoka, Selective delivery of adriamycin to a solid tumor using a polymeric micelle carrier system, J. Drug Target. 7 (1999) 171–186.
[29] G. Cavaletti, G. Tredici, M.G. Petruccioli, E. Donde, P. Tredici, P. Marmiroli, C. Minoia, A. Ronchi, M. Bayssas, G. Griffon Etienne, Effects of different schedules of oxaliplatin treatment on the peripheral nervous system of the rat, Eur. J. Cancer 37 (2001) 2457–2463.
[30] F. Grolleau, L. Gamelin, M. Boisdron-Celle, B. Lapied, M. Pelhate, E. Gamelin, A possible explanation for a neurotoxic effect of the anticancer agent oxaliplatin on neuronal voltage-gated sodium channels, J. Neurophysiol. 85 (2001) 2293–2297.
[31] L. Rubbia-Brandt, V. Audard, P. Sartoretti, A.D. Roth, C. Brezault, M. Le Charpentier, B. Dousset, P. Morel, O. Soubrane, S. Chaussade, G. Mentha, B. Terris, Severe hepatic sinusoidal obstruction associated with oxaliplatin based chemotherapy in patients with metastatic colorectal cancer, Ann. Oncol. 15 (2004) 460–466.
[32] G. Tisman, D. MacDonald, N. Shindell, E. Reece, P. Patel, N. Honda, E.K. Nishimora, J. Garris, W. Shannahan, N. Chisti, J. McCarthy, S.N. Moaddeli, D. Sargent, A. Plant, Oxaliplatin toxicity masquerading as recurrent colon cancer, J. Clin. Oncol. 22 (2004) 3202–3204.
[33] J. Liu, E. Kraut, J. Bender, R. Brooks, S. Balcerzak, M. Grever, H. Stanley, S. D'Ambrosio, R. Gibson-D'Ambrosio, K.K. Chan, Pharmacokinetics of oxaliplatin (NSC266046) alone and in combination with paclitaxel in cancer patients, Cancer Chemother. Pharmacol. 49 (2002) 367–374.
[34] C. Massari, S. Brienza, M. Rotarski, J. Gastiaburu, J.-L. Misset, D. Cupissol, E. Alafaci, H. Dutertre-Catella, G. Bastian, Pharmacokinetics of oxaliplatin in patients with normal versus impaired renal function, Cancer Chemother. Pharmacol. 45 (2000) 157–164.
[35] F.R. Luo, S.D. Wyrick, S.G. Chaney, Biotransformations of oxaliplatin in rat blood *in vitro*, J. Biochem. Molec. Toxicol. 13 (1999) 159–169.
[36] F.R. Luo, T.-Y. Yen, S.D. Wyrick, S.G. Chaney, High-performance liquid chromatographic separation of the biotransformation products of oxaliplatin, J. Chromatogr., B 724 (1999) 345–356.
[37] F.R. Luo, S.D. Wyrick, S.G. Chaney, Cytotoxicity, cellular uptake and cellular biotransformations of oxaliplatin in human colon carcinoma cells, Oncol. Res. 10 (1998) 595–603.
[38] E. Jerremalm, P. Videhult, G. Alvelius, W.J. Griffiths, T. Bergman, S. Eksborg, H. Ehrsson, Alkaline hydrolysis of oxaliplatin — isolation and identification of the oxalato monodentate intermediate, J. Pharm. Sci. 91 (2002) 2116–2121.

Available online at www.sciencedirect.com
ScienceDirect
Journal of Controlled Release 121 (2007) 38–48
journal of controlled release
www.elsevier.com/locate/jconrel

Transfection study using multicellular tumor spheroids for screening non-viral polymeric gene vectors with low cytotoxicity and high transfection efficiencies

Muri Han [a], Younsoo Bae [b,c], Nobuhiro Nishiyama [b,c,d], Kanjiro Miyata [c,e], Makoto Oba [f], Kazunori Kataoka [a,b,c,d,e,*]

[a] Department of Materials Engineering, School of Engineering, The University of Tokyo, 7-3-1 Hongo, Bunkyo-ku, Tokyo 113-8656, Japan
[b] Center for Disease Biology and Integrative Medicine, School of Medicine, The University of Tokyo, 7-3-1 Hongo, Bunkyo-ku, Tokyo 113-0033, Japan
[c] Center for NanoBio Integration, The University of Tokyo, 7-3-1 Hongo, Bunkyo-ku, Tokyo 113-8656, Japan
[d] Core Research for Evolutional Science and Technology (CREST), Japan Science and Technology Agency (JST), Japan
[e] Department of Bioengineering, School of Engineering, The University of Tokyo, 7-3-1 Hongo, Bunkyo-ku, Tokyo 113-0033, Japan
[f] Department of Clinical Vascular Regeneration, School of Medicine, The University of Tokyo, 7-3-1 Hongo, Bunkyo-ku, Tokyo 113-8655, Japan

Received 19 March 2007; accepted 8 May 2007
Available online 17 May 2007

Abstract

Polyplexes consisting of plasmid DNA and polycations have received much attention as promising vectors for gene transfer. For effective gene therapy, polycations with different polyamine structures in the side chain were developed to ensure their buffering capacity for endosomal escape, and their PEGylated block copolymers were developed to increase their stability and biocompatibility. The effects of the chemical structures of polycations and their PEGylation on transfection and cytotoxicity were elucidated by use of a three-dimensional multicellular tumor spheroid of human hepatoma HuH-7 cells. Various features of transfection with polyplex micelles, which have been hard to observe in conventional monolayer cultures, were revealed by the multicellular tumor spheroid (MCTS) model in terms of cytotoxicity and time-dependent behaviors of transfected gene expression under three-dimensional microenvironments. By using this system, the polyplex micelle from poly(ethylene glycol)-*b*-poly(*N*-substituted asparagine) copolymers having the *N*-(2-aminoethyl)-2-aminoethyl group in the side chain (PEG-*b*-P[Asp(DET)] polyplex micelle) was proved to achieve high transfection efficiencies as well as low cytotoxicity, both of which are critical properties for successful in vivo gene delivery.

Keywords: Non-viral gene vector; Block copolymer; Polyplex micelle; Spheroid

1. Introduction

A variety of non-viral polymeric gene vectors have received much attention in the past decade [1–3] for the delivery of genetic materials to the targeted cells in an effective and safe manner. Especially, the polyplexes formed by the electrostatic interaction between plasmid DNA (pDNA) and polycations have been designed to condense pDNA by shielding its negative charges, protect pDNA from rapid nucleolytic degradation, and facilitate its cellular uptake in order to achieve effective gene delivery [4–6]. It is well known that the chemical structures of polycations in polyplex systems play important roles in transfection efficiency. In this regard, polyethylenimine (PEI)-based polyplexes have been shown to be highly transfectable, presumably through the buffering of the endosomal cavity (i.e., so-called proton sponge effect) [2]. One of the advantages of polyplex systems is the possibility of various structural modifications to improve the stability and transfection efficiency of the polyplexes. Among such modifications, PEGylation [modification with poly(ethylene glycol)(PEG)] of polycations is a promising way to realize systemic gene delivery due to the improved stability of polyplexes in biological media [7–10].

* Corresponding author. Department of Materials Engineering, Graduate School of Engineering, The University of Tokyo, 7-3-1 Hongo, Bunkyo-ku, Tokyo 113-8656, Japan. Fax: +81 3 5841 7139.
E-mail address: kataoka@bmw.t.u-tokyo.ac.jp (K. Kataoka).

0168-3659/$ - see front matter © 2007 Elsevier B.V. All rights reserved.
doi:10.1016/j.jconrel.2007.05.012

A typical PEGylated polyplex is a core-shell type polyplex (polyplex micelle) formed through the electrostatic interaction between pDNA and PEG-*block*-polycation copolymers. Polyplex micelles have been demonstrated to show high colloidal stability under biological media and substantial transfection activity against various cells even after preincubation with serum proteins [11,12]. Moreover, polyplex micelles showed prolonged blood circulation and in vivo gene transfer to liver [5,13]. The chemical structures of polycations in block copolymers substantially affect the capability of polyplexes as efficient gene vectors. In this regard, we recently reported the development of highly transfectable but remarkably low cytotoxic PEG-*block*-polycation copolymers: PEG-*b*-poly(*N*-substituted asparagine) copolymers having the *N*-(2-aminoethyl)-2-aminoethyl group in the side chain (PEG-*b*-P[Asp(DET)]) [14]. Polyplex micelles from PEG-*b*-P[Asp(DET)] showed efficient and non-toxic transfection to several primary cells including endothelial and smooth muscle cells, which are sensitive to the polyplex-induced cytotoxicity, and successful gene transfection in vivo to vascular lesions [15]. Thus, the PEG-*b*-P[Asp(DET)] polyplex micelle is expected to be a potent non-viral vector for in vivo gene delivery.

The unique feature of the PEG-*b*-P[Asp(DET)] polyplex micelle to achieve appreciably high transfection efficacy with substantially lowered toxicity motivated us to further clarify the effects of PEGylation and the chemical structures of polyasparagine-based polyplexes on their transfection and cytotoxic behaviors. For this purpose, we have compared here two types of polyasparagine-based polycations having a subtle difference in the number of methylene units in the side chain: *N*-(2-aminoethyl)-2-aminoethyl group (P[Asp(DET)]) and *N*-(3-aminopropyl)-3-aminopropyl group (P[Asp(DPT)]). Furthermore, to explore the effect of PEGylation on polyplex behavior, two types of PEG-*b*-cationic polyasparagines, PEG-*b*-P[Asp(DET)] and PEG-*b*-P[Asp(DPT)], were prepared for the construction of polyplex micelles (Scheme 1). The transfection activity and cytotoxicity of polyplexes and polyplex micelles were evaluated with multicellular tumor spheroids (MCTS) as well as conventional monolayer culture cells. We focus on MCTS here because they are known to be very useful three-dimensional in vitro tumor models, representing morphological and functional features of in vivo avascular solid tumors, and because they are characterized by prolonged viable spans with actively proliferating outer cell layers [16]. Recently, Mellor et al. applied the transfection of polyethylenimine-based polyplexes to the MCTS with the relatively large size (~474 μm) to assess the penetration of the polyplexes inside the spheroids, approaching the issue of polyplex percolation in actual in vivo tissues [17]. In the present study, we focused on the MCTS with the relatively small size due to our finding that the size of MCTS is highly sensitive to polyplex-induced cytotoxicity; MCTS of approximately 100 μm showed even higher sensitivity than monolayered culture cells, probably due to their immature development of cell–cell and cell–extracellular matrix (ECM) interactions. Worth noting is that the prolonged viable span of MCTS allowed long-term evaluation of more than 10 days of the expression of transfected genes. These properties of MCTS models enabled us to evaluate polyplex systems under conditions close to those of in vivo solid tumors, revealing the excellent biocompatibility and durable gene expression behaviors of PEG-*b*-P[Asp(DET)] polyplex micelles.

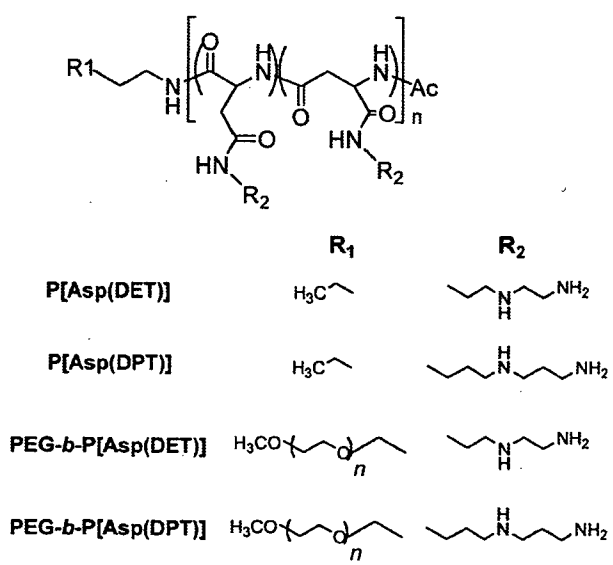

Scheme 1. Chemical structures of polycations.

2. Experimental

2.1. Materials

β-Benzyl-L-aspartate *N*-carboxyanhidride (BLA-NCA) and α-methoxy-ω-amino poly(ethylene glycol) (MeO-PEG-NH_2) (M_r=12,000) were obtained from Nippon Oil and Fats Co., Ltd. (Japan). Diethylenetriaimine (DET) and dipropylenetriamine (DPT) were purchased from Tokyo Kasei Kogyo Co., Ltd. (Japan) and distilled over CaH_2 under reduced pressure. *N*,*N*-Dimethylformamide (DMF), dichloromethane, and acetic anhydride were purchased from Wako Pure Chemical Industries, Ltd. (Japan) and purified by general methods before use. Linear polyethylenimine (ExGen 500 in vitro transfection reagent, 22 KDa) and branched polyethylenimine (25 KDa) were purchased from Fermentas (Canada) and Aldrich (USA), respectively.

2.2. Synthesis of poly(N-substituted asparagines) and their block copolymers with poly(ethylene glycol) (PEG)

The PEG-*block*-poly(β-benzyl L-aspartate) (PEG-*b*-PBLA) was prepared as previously reported [14]. Briefly, BLA-NCA was polymerized in DMF at 40 °C from the terminal primary amino group of MeO-PEG-NH_2, followed by the acetylation of the *N*-terminus of PBLA by acetic anhydride to obtain PEG-*b*-PBLA-Ac. PEG-*b*-PBLA-Ac was confirmed to have a unimodal molecular weight distribution (M_w/M_n: 1.17) by gel-permeation chromatography (GPC) measurement [columns: TSK-gel G4000HHR+G3000HHR, eluent: DMF+10 mM LiCl, T=40 °C, detector: Refractive Index (RI)] (data not shown).

The degree of polymerization (DP) of PBLA was calculated to be 101 based on ^{1}H NMR spectroscopy (data not shown).

Lyophilized PEG-*b*-PBLA (300 mg, 11.6 μmol) was dissolved in DMF (10 mL), followed by the reaction with DET (50 equiv to benzyl group of PBLA segment, 4.0 g, 39.4 mmol) under mild anhydrous conditions to obtain PEG-*b*-P[Asp(DET)]. After 24 h, the reaction mixture was slowly added dropwise into a solution of acetic acid (10% *v/v*, 40 mL) and dialyzed against a solution of 0.01 N HCl and then distilled water (M_r cutoff: 3500 Da). The final solution was lyophilized to obtain the polymer as the chloride salt form, and the yield was approximately 90%. Similarly, PEG-*b*-P[Asp(DPT)] was synthesized by the aminolysis reaction of PEG-*b*-PBLA-Ac with DPT. The structures of these block catiomers were confirmed by ^{1}H and ^{13}C NMR measurements.

Cationic homopolymers, P[Asp(DET)] and P[Asp(DPT)], were synthesized by the aminolysis reaction of PBLA homopolymer [degree of polymerization (DP): 98], which was obtained by the polymerization of BLA-NCA initiated by *n*-butylamine. The unimodal distribution and the almost 100% conversion of the BLA side chains of these homopolymers into the desired amino groups were confirmed by GPC and ^{1}H NMR measurements, respectively.

2.3. Titration of polymers

Each homopolymer (68 mg of P[Asp(DET)] and 75 mg of P[Asp(DPT)]) or block copolymer (98 mg of PEG-*b*-P[Asp(DET)] and 104 mg of PEG-*b*-P[Asp(DPT)]) was dissolved in 40 mL of 0.005 N HCl with 150 mM NaCl, and titrated with 0.05 N NaOH with 150 mM NaCl at 37 °C. An automatic titrator (TITSTATION TS-2000, Hiranuma Co., Ltd., Kyoto, Japan) was used for the titration. In this experiment, the titrant was added in 0.0315 mL quantities after the confirmation that the pH values became stable (minimal interval: 30 s). The pH-α curves were determined from the obtained titration curve. For the estimation of the charge in the protonation affinity with α apparent $pK(=pH+\log[\alpha/(1-\alpha)])$ was plotted against $1-\alpha$, where K is the effective dissociation constant.

2.4. Plasmid DNA

The plasmid, pCAcc vector having CAG promoter [18], was provided by RIKEN Bioresource Center (Japan). Also, a fragment cDNA of SEYFP-F46L (*Venus*), which is a variant of yellow fluorescent protein with the mutation F46L [19], was provided by Dr. A. Miyawaki at the Brain Science Institute, RIKEN (Japan) and inserted into the pCAcc vector (pCAcc+*Venus*). Each plasmid DNA (pDNA) was amplified in competent DH5α *Escherichia coli* and purified using HiSpeed Plasmid MaxiKit (QIAGEN Sciences Co., Inc., Germany). The pDNA concentration was determined by the absorption at 260 nm.

2.5. Preparation of the polyplexes

Poly(ethylene glycol)-*block*-polycation copolymer and pDNA were first separately dissolved in 10 mM Tris–HCl buffer (pH 7.4). Then, both solutions were mixed at various ratios of the number of amino group (primary and secondary amino groups) units per nucleotide (*N/P* ratios). The final pDNA concentration of the mixture was adjusted to 100 μg/mL. Polyplex micelle was applied to each well for transfection after overnight incubation at ambient temperature. Polyplex was prepared similarly by mixing cationic homopolymer and pDNA solution. Polyplex was applied to each well for transfection after 30 min of incubation at ambient temperature.

2.6. In vitro transfection to HuH-7 cells

For the monolayer culture study, human hepatoma HuH-7 cells were seeded on 24-well culture plates and incubated overnight in 400 μL of Dulbecco's modified eagle's medium (DMEM) containing 10% fetal bovine serum (FBS) before transfection. Then, 10 μL of each polyplex solution was applied to each well for the transfection. The amount of pDNA was adjusted to 1 μg per well. After 24 h of incubation, the medium was replaced with 400 μL of the medium containing 10% serum, followed by an additional 24 h of incubation. The luciferase gene expression was then evaluated using the Luciferase Assay System (Promega, USA) and a Lumat LB9507 luminometer (Berthold Technologies, Germany). The amount of protein in each well was concomitantly determined using a Micro BCA Protein Assay Reagent Kit. To prepare MCTS, 200 μL of cell suspension (2×10^2 cell/ml) was seeded into a 96-well culture plate designed for spheroid formation (SUMILONCELLTIGHT, Sumitomo Bakelite Co., Ltd., Japan). After 48 h of incubation, a multicellular spheroid with diameter of ca 100 μm was spontaneously formed in each well. Then, 10 μL of each polyplex solution was applied to each well for the transfection. The amount of pDNA was adjusted to 1 μg per well. After 24 h of incubation, the medium was replaced with 200 μL of the medium containing 10% serum, followed by an additional 24 h of incubation. During the incubation period, the medium was replaced by fresh medium containing 10% serum every 3 days. The *Venus* gene expression was then evaluated using an LSM 510 confocal microscope (Carl Zeiss, Germany; excitation wavelength: 488 nm).

2.7. Live/dead assay

Live and Dead assay was accomplished with the Live/Dead kit protocol (Molecular Probes, USA) against cultured spheroids. Spheroids were rinsed with PBS (−) and then incubated with a solution containing 0.8 μM calcein AM (excitation 495 nm, emission 515 nm) and 4 μM EthD-1 (excitation 495 nm, emission 635 nm) in PBS (−) for 3 h at 37 °C, followed by observation through a Carl Zeiss LSM 510 confocal laser scanning microscope. The concentration and incubation time were optimized to allow the selective labeling of HuH-7 spheroids between live and dead cells.

2.8. Fluorescence measurements

For observation of the gene expression of the fluorescent protein *Venus*, MCTS samples were rinsed and mounted in PBS (−), and then observed by confocal microscope. The LSM 510

laser scanning microscope was used for the optical sectioning of the spheroids. An argon gas laser with an excitation wavelength of 488 nm was used to emit the fluorescence of the YFP.

2.9. Cell viability assay

Cell viability assay was accomplished with a protocol (CellTiter-Glo®Luminescent Cell Viability Assay, Promega, USA) against cultured cells. After 24 h incubation of HuH-7 cells in opaque 24-well plates, the polyplex to be tested was added. The cells were rinsed with PBS (−) after 24 h of incubation, then 200 μL of reagent to an equal volume of cell culture medium was added to each well. After mixing for 2 min, the plate was incubated at room temperature for 10 min. The luminescence was evaluated using a Lumat LB9507 luminometer (Berthold Technologies, Germany).

2.10. Quantification of gene expression in MCTS

The total intensity was calculated from the piled up fluorescence images of fluorescence of *Venus* from each optical slice (at a depth of 1 μm) by Imaris® software in combination with Imaris MeasurementPro (Carl Zeiss, Germany), which enables the measurement of the intensity value for groups of selected voxels. The relative intensity was determined from the total intensity of one spheroid divided by a volume of spheroid.

2.11. Dissociation of P[Asp(DET)] polyplex and PEG-b-P[Asp(DET)] micelle

The release of pDNA from the complexes was evaluated through the exchange reaction with an anionic lipid, 1,2-dioleoyl-*sn*-glycero-3-phospho-L-serine sodium salt (DOPS, Sigma). Two mg/mL of DOPS solution was added to the P[Asp(DET)] polyplex and to the PEG-*b*-P[Asp(DET)] polyplex micelle solutions prepared at the *N/P* ratio of 20 to obtain mixed solutions with varying unit molar ratios ([carboxyl groups in DOPS]/[phosphate groups in pDNA]). The final pDNA concentration was adjusted to 16.7 μg/mL. After overnight incubation at 25 °C, the mixed solutions were electrophoresed with 0.9 wt.% agarose gel in the buffer (3.3 mM Tris–acetic acid (pH 7.4)+1.7 mM sodium acetate+1 mM EDTA2Na). pDNAs in the gel were visualized by soaking the gel in an ethidium bromide solution (0.5 mg/L) and analyzed using a Luminous Imager V5 (AISIN SEIKI Co., Ltd., Japan).

3. Results

3.1. Protonation behaviors of polycations and their block copolymers with PEG

In this study, sets of cationic poly(*N*-substituted asparagine) homopolymers and PEG-*b*-poly(*N*-substituted asparagine) copolymers having the *N*-(2-aminoethyl)-2-aminoethyl group (P[Asp(DET)]) or the *N*-(3-aminopropyl)-3-aminopropyl group (P[Asp(DPT)]) in the side chain (Scheme 1) were prepared to study the effects of the chemical structures of polycations as well as the PEGylation of polycations on the properties of polyplex components. This synthetic method is based on our finding that the flanking benzyl ester groups of PBLA undergo a quantitative aminolysis reaction with various polyamine compounds under careful anhydrous conditions, so that a series of polymers has the same polymerization degree and distribution [14], allowing a direct comparison of subtle changes in their chemical structures.

The pH-dependent protonation behaviors of the obtained homopolymers, P[Asp(DET)] and P[Asp(DPT)], in 150 mM NaCl-containing media at 37°C seemed to be clearly distinct as shown in Fig. 1A. Indeed, P[Asp(DET)] displayed two-step protonation behavior and the protonation degree (α) of 0.53 at pH 7.4, whereas the protonation of P[Asp(DPT)] did not show clear two-step protonation and showed a higher protonation degree (α=0.88) at pH 7.4. From the p*K*–α curve (data not shown), the pK_1 (p*K* at α=0.25) and pK_2 (p*K* at α=0.75) of P[Asp(DET)] were calculated as 9.1 and 6.3, respectively, and the pK_1 and pK_2 of P[Asp(DPT)] were also calculated as 9.7 and 8.6, respectively. The two distinct p*K* values (pK_1 and pK_2) correspond to the first and

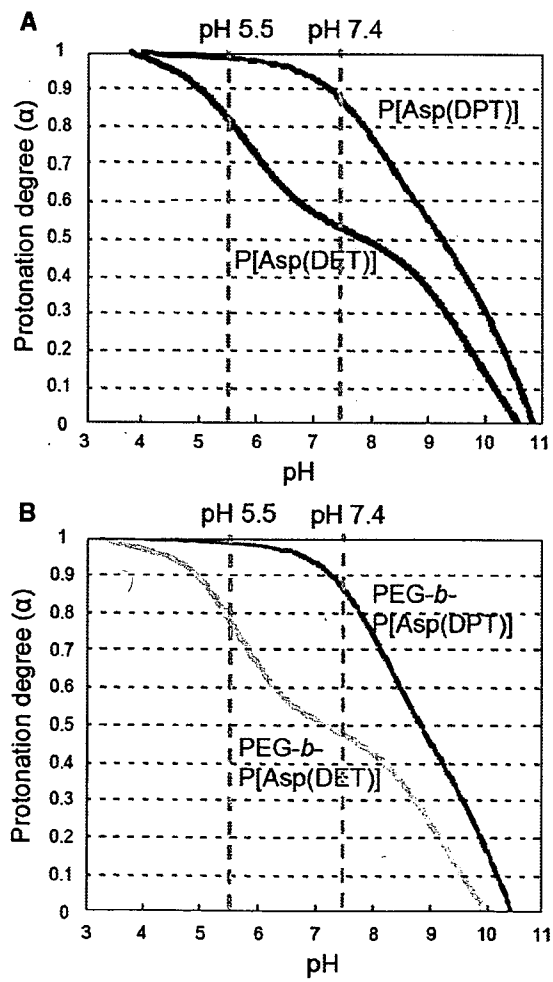

Fig. 1. pH–α (protonation degree) curves of P[Asp(DET)] and P[Asp(DPT)] (A) and PEG-*b*-P[Asp(DET)] and PEG-*b*-P[Asp(DPT)] (B) (37 °C, 150 mM NaCl, 0.05 M NaOH as titrant, 0.5 mmol amine concentration).

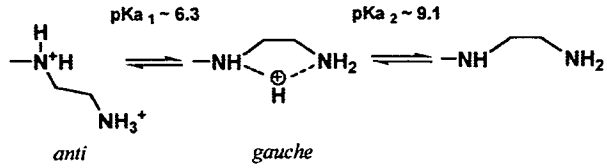

Scheme 2. Two-step protonation of ethylenediamine side chain of P[Asp(DET)].

second protonation steps of diamine units, respectively, in the side chain. Consequently, P[Asp(DET)] might exert a substantial buffering capacity in the pH range from 7.4 to 5.0, leading presumably to potent transfection activity based on the proton sponge effect. It is noteworthy that P[Asp(DET)] has a two orders of magnitude higher proton dissociation constant (or lower protonation constant) for the second protonation than P[Asp(DPT)], indicating that the former is less favorable than the latter to the double-protonated state. This may be due to the strong electrostatic repulsion between two protonated amines in ethylenediamine units of P[Asp(DET)] to take only the *anti*-conformation (Scheme 2). As seen in the case of P[Asp(DPT)], an increase in one more unit of the methylene group between two amino groups in the side chain effectively reduces the electrostatic repulsion to facilitate the protonation.

pH-α curves of PEG-*b*-poly(*N*-substituted asparagine) (PEG-*b*-P[Asp(DET)] and PEG-*b*-P[Asp(DPT)]) were also shown in Fig. 1B, showing a tendency similar to those of the homopolymers in Fig. 1A. From these results, the pK_1 and pK_2 of PEG-*b*-P[Asp(DET)] were calculated as 8.5 and 6.2, whereas the pK_1 and pK_2 of PEG-*b*-P[Asp(DPT)] were calculated as 9.3 and 8.5, respectively. It is noted that PEGylation of the polycations decreased the p*K* values, suggesting that PEGylation might prevent the protonation of polycations. Presumably, this might be explained by the decrease in the local permittivity of polycations caused by surrounding PEG chains.

3.2. Transfection efficiencies and cytotoxicity of polyplexes against monolayer cultured cells

The transfection efficiencies of cationic homopolymers/pDNA polyplexes against monolayer cultured HuH-7 cells were evaluated. The results of transfection after 48 h incubation (24 h incubation with the polyplexes followed by 24 h post-incubation after medium replacement) are shown in Fig. 2A. P[Asp(DET)] polyplexes showed high transfection efficiencies over the range of *N/P* ratios tested in this study. Especially, they displayed comparable or even higher transfection efficiencies at *N/P*=20 and 40 compared with LPEI and BPEI polyplexes [*N/P*=6 for LPEI according to the manufacturer's recommendation and *N/P*=10 for BPEI by optimization], which have been widely used in experimental transfection. P[Asp(DPT)] polyplexes showed appreciable transfection efficiency at *N/P*=10; however, the efficiency decreased at *N/P*=20 and 40, probably due to the emergence of significant cytotoxicity (Fig. 3).

Regarding the cytotoxicity of the polyplexes from cationic homopolymers (Fig. 3), both LPEI and BPEI polyplexes induced significant decreases in cell viability even at the *N/P* ratio appropriate for transfection. Polyplexes from P[Asp(DET)] were significantly less cytotoxic than the other polyplexes, whereas P[Asp(DPT)] polyplexes turned out to be highly cytotoxic. Thus, a subtle change in the chemical structure of the side chain of poly(*N*-substituted asparagine) unprecedentedly affected the cytotoxicity of the polyplexes.

In the cases of polyplex micelles from the block catiomers, PEG-*b*-P[Asp(DET)] polyplex micelles showed much better transfection efficiencies than PEG-*b*-P[Asp(DPT)] polyplex micelles (Fig. 2B), as was the case with the polyplexes from the corresponding homopolymers. With an increase in *N/P* ratio, each polyplex micelle showed an increase in transfection activity. Regarding cytotoxicity (Fig. 3), the PEG-*b*-P[Asp(DET)] polyplex micelles always displayed lower cytotoxicity than the

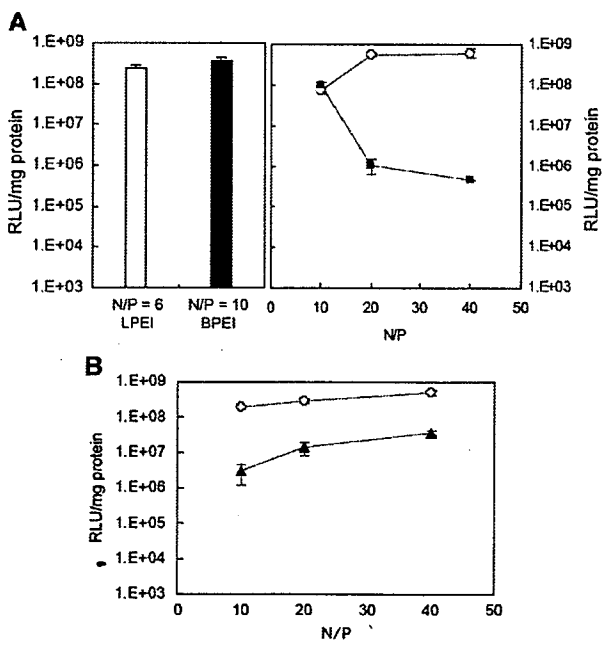

Fig. 2. The transfection of luciferase reporter gene against monolayer cultures of HuH-7. A) Transfection results with L/BPEI polyplexes (*N/P*=6 for LPEI according to the manufacturer's recommendation and *N/P*=10 for BPEI by optimization), P[Asp(DET)] polyplexes (○) and P[Asp(DPT)] polyplexes (■). B) Transfection results with PEG-*b*-P[Asp(DET)] polyplex micelles (○) and PEG-*b*-P[Asp(DPT)] polyplex micelles (▲).

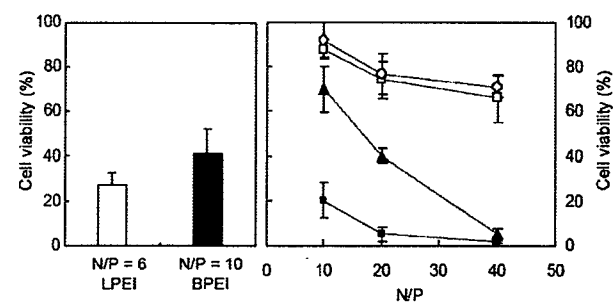

Fig. 3. Cytotoxicity of L/BPEI polyplexes (*N/P*=6 for LPEI according to the manufacturer's recommendation and *N/P*=10 for BPEI by optimization), P[Asp(DET)] polyplexes (□), P[Asp(DPT)] polyplexes (■), PEG-*b*-P[Asp(DET)] polyplex micelles (○), and PEG-*b*-P[Asp(DPT)] polyplex micelles (▲) toward HuH-7 cells after 48 h incubation.

PEG-*b*-P[Asp(DPT)] polyplex micelles at the same *N/P* ratios, and the difference in their cytotoxicity between these polyplex micelles became progressively more significant with increases in the *N/P* ratios. The cell viability remained high, and at levels similar between P[Asp(DET)] polyplexes and PEG-*b*-P[Asp (DET)] polyplex micelles, even with increased *N/P* ratios. This result suggests that the P[Asp(DET)] structure may have an inherently low cytotoxicity, which was further confirmed by the cytotoxicity assay of free polymers (Supporting Information 1). Notably, PEGylation significantly decreased the cytotoxicity of P[Asp(DPT)], resulting in improved transfection efficacy particularly at higher *N/P* ratios. This result clearly indicates that PEGylation is an efficient way to improve the compliance of a polyplex system involving cytotoxic polycations as a component [20]. Nevertheless, the PEGlyation of P[Asp(DET)] did not show any significant effect on cytotoxicity, apparently due to the minimally cytotoxic nature of the P[Asp(DET)] structure.

3.3. Evaluation of characteristic properties of MCTS

Fig. 4 shows the growth of HuH-7 MCTS from the initial diameter of 100 μm. By using Live/Dead assay (live cells: green fluorescence; dead cells: red fluorescence), necrosis of the inner cells of MCTS was observed by a confocal laser scanning microscope (CLSM) when the diameter reached around 400–500 μm (6–8 days after incubation). The necrotic region expanded along with the growth of MCTS. Thus, HuH-7 MCTS clearly took a heterogeneous structure according to the distance from the outer cell layers after they grew beyond the diffusion limit of oxygen and nutrition. Such a growth property represents a good in vitro model for the heterogeneity of solid tumors as a result of the inefficient vascular function [21,22].

3.4. Transfection efficiencies and cytotoxicity of polyplexes and polyplex micelles against MCTS

The gene expression of fluorescent protein *Venus* at defined time periods after transfection with the polyplexes or polyplex micelles was observed by CLSM as shown in Fig. 5. The spheroid diameter at the time of transfection was adjusted to 100 μm to ensure the long-term observation of the transfected gene expression within the optically observable depth range by CLSM. Under this condition, gene expression continued for over 10 days after the transfection and in some cases continued for over 1 month (data not shown). Images of the localization of transfected protein *Venus* in MCTS were taken from the upper surface going towards the center of the MCTS by the z-axis at 1–2 μm intervals of optical slices. Fig. 5A shows typical images of transfected *Venus* in MCTS at different *z*-axes (different distances from the spheroid surface) at 8 days after transfection with PEG-*b*-P[Asp(DET)] polyplex micelles (*N/P*=40). The images clearly showed that *Venus* was expressed even at the inner region of MCTS where necrosis was considered to be developed at the corresponding size (Fig. 4).

All the MCTS structures were destroyed after transfection with LPEI or BPEI polyplexes due to their toxicity even at low

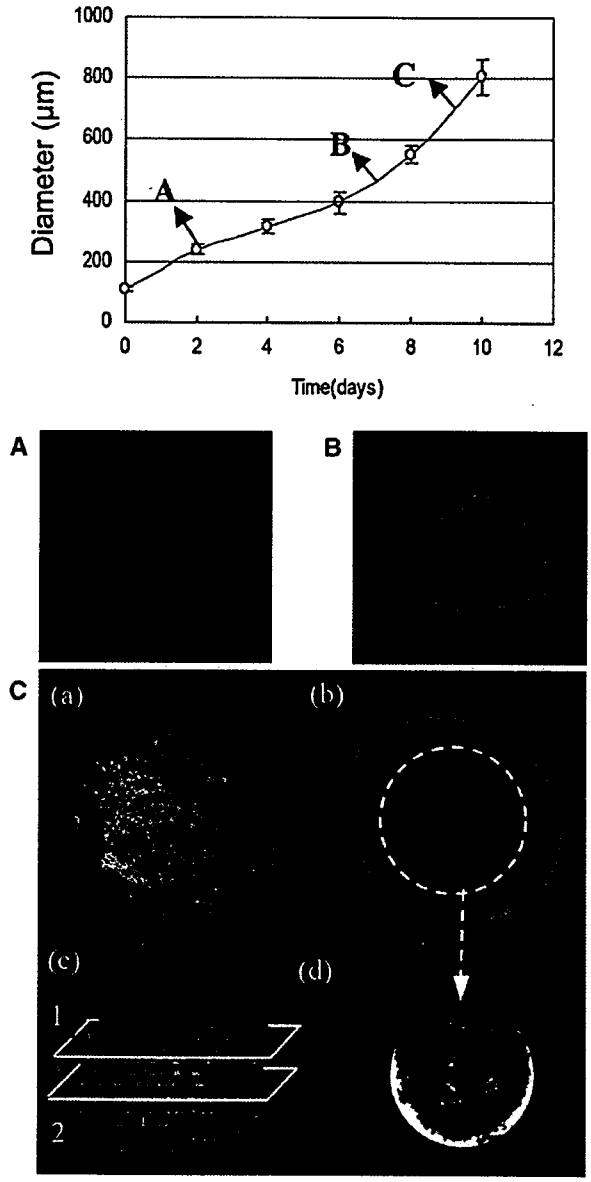

Fig. 4. Growth curve of HuH-7 spheroids and Live/Dead assay of spheroid at each time point of incubation (initial diameter is ca 100 μm. Optical slice at the middle of spheroid. Bar=100 μm. Green and red fluorescence from live and dead cells, respectively). A) 2 days after the formation of MCTS. B) 7 days after the formation of MCTS. C) 9 days after the formation of MCTS. In C, (a) optical slice of spheroid at position 1 of (c); (b) optical slice of spheroid at position 2 of (c); (c) side view of spheroid*; (d) retaken image of region of interest (ROI)**. (*This image was constructed by piling up side views. **This image was taken by stimulating the radiation of ROI by the amplification of laser.)

N/P ratios, and thus no systematic data on the spheroid transfection were obtained. P[Asp(DPT)] polyplexes also induced the destruction of MCTS in the whole range of *N/P* ratios tested in this study (*N/P*=10, 20, and 40). By contrast, P [Asp(DET)] polyplexes showed successful transfection without destruction of the MCTS structure at *N/P* ratios of 10 and 20, as seen in Fig. 5B, highlighting the lower cytotoxicity of P[Asp (DET)] compared with P[Asp(DPT)], LPEI, and BPEI. Here,

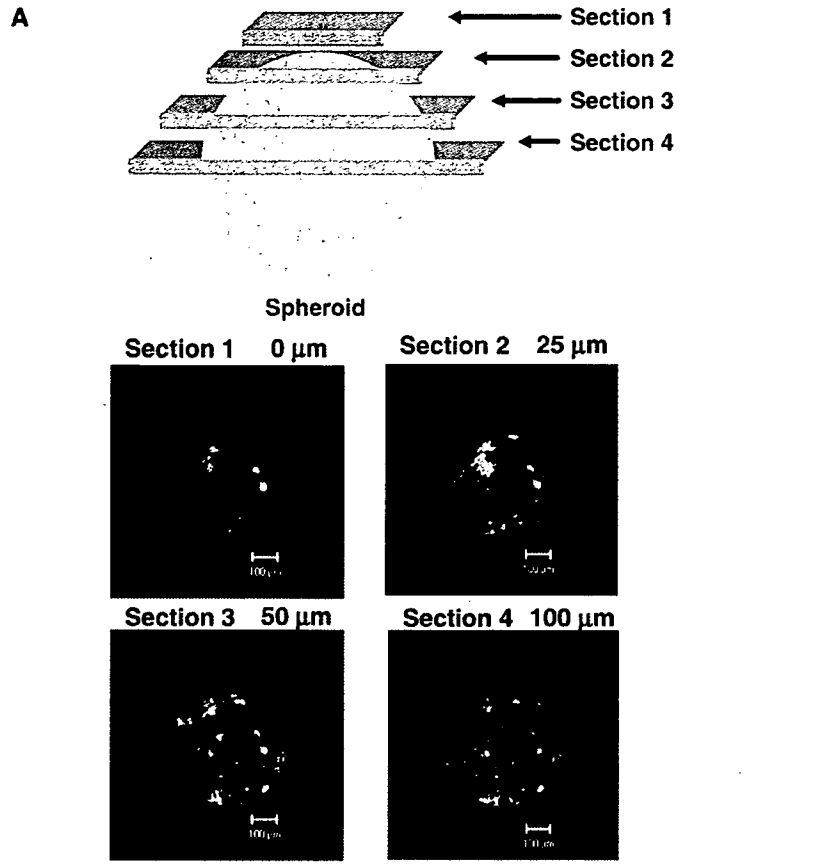
A
Section 1
Section 2
Section 3
Section 4
Spheroid
Section 1 0 μm
Section 2 25 μm
Section 3 50 μm
Section 4 100 μm
B
LPEI
N/P
6
BPEI
10
P[Asp(DET)]
10
20
40
P[Asp(DPT)]
10, 20, 40
2 days
4 days
6 days
8 days
10 days
No data due to MCTS destruction
No data due to MCTS destruction
No data due to MCTS destruction
No data due to MCTS destruction

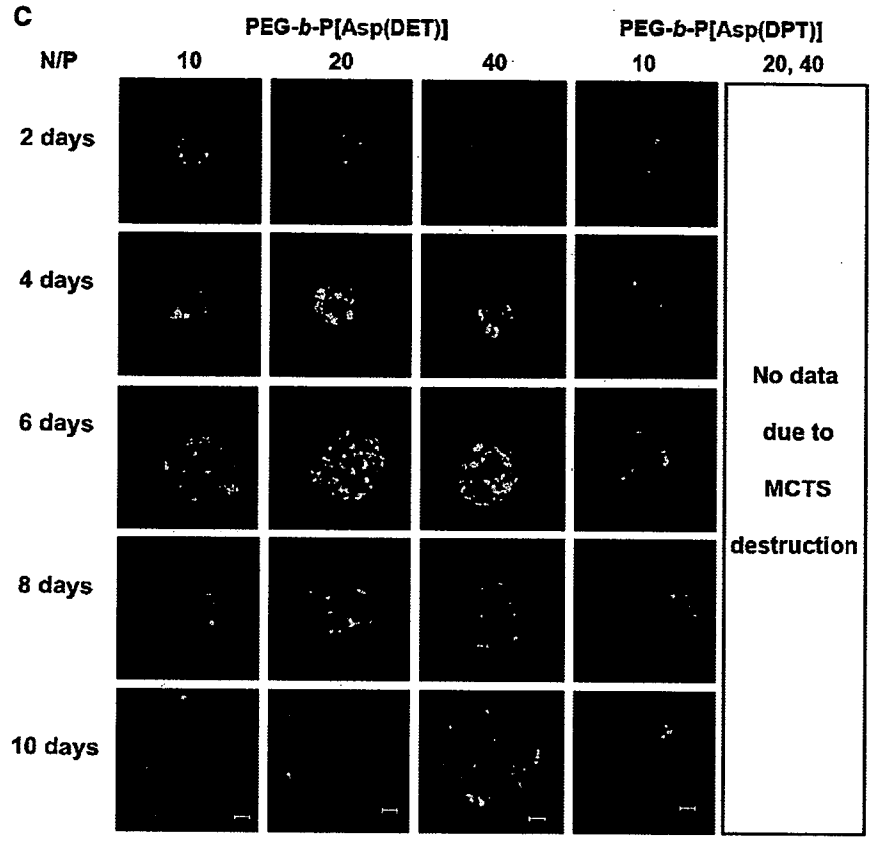

Fig. 5. Expression of marker protein *Venus* in HuH-7 spheroids (initial diameter is ca 100 μm. Bar=100 μm). A) Localization of transfected *Venus* by PEG-*b*-P[Asp(DET)] polyplex micelles according to the distance from the surface of the spheroid. (The images were the optical slices taken from the upper surface toward the center of the MCTS by the *z*-axis at 0, 25, 50, and 100 μm). B) Optical slices at the middle of spheroids with transfected protein *Venus* by P[Asp(DET)] and P[Asp(DPT)] polyplexes. (Results were not obtained due to the destruction of spheroids after transfection in the cases of *N/P*=4, 6, 8, 10 for LPEI, *N/P*=10, 20, 40 for BPEI, *N/P*=40 for P[Asp(DET)], *N/P*=10, 20, 40 for P[Asp(DPT)]). C) Optical slices at the middle of spheroids with transfected protein *Venus* by PEG-*b*-P[Asp(DET)] and PEG-*b*-P[Asp(DPT)] polyplex micelles. (Results were not obtained due to the destruction of spheroids after transfection in the cases of *N/P*=20, 40 for PEG-*b*-P[Asp(DPT)].)

the MCTS images at the middle section by the *z*-axis are shown for each day period. However, even P[Asp(DET)] polyplexes showed the destruction of spheroid structures by increasing the *N/P* ratio to 40.

Overall, PEG-*b*-P[Asp(DET) polyplex micelles showed better transfection activity than PEG-*b*-P[Asp(DPT)] polyplex micelles in MCTS, in agreement with the results of monolayer culture (Fig. 2B). PEG-*b*-P[Asp(DET)] polyplex micelles showed successful activity of the transfection without destruction of MCTS across the range of *N/P* ratios tested in this study (*N/P*=10, 20, and 40) (Fig. 5C). Worth mentioning is that PEG-*b*-P[Asp(DET)] polyplex micelles did not induce the destruction of spheroids even at *N/P*=40, where the MCTS structures were destroyed by the transfection with P[Asp(DET)] polyplexes (Fig. 5B) at that *N/P* ratio. Such reduction of cytotoxicity by PEGylation of polycations were not detected by the conventional monolayer culture study (Fig. 3, Supporting Information 1), highlighting high sensitivity of MCTS against polyplex-induced cytotoxicity. While the transfection efficiency of P[Asp(DPT)] was not obtained due to the destruction of MCTS after the transfection, the effect of PEGylation on reducing toxicity was remarkable in this case. Eventually, PEG-*b*-P[Asp(DPT)] polyplex micelles showed appreciable transfection efficiency at the *N/P* ratio of 10.

3.5. Time-dependent gene expression in MCTS

The total fluorescence intensity by *Venus* expression in MCTS was calculated by integrating the intensity image of each optical slice taken from the upper surface going towards the center of the MCTS by the *z*-axis at 1–2 μm intervals (Fig. 5A) using Imaris® software (Fig. 6A). The gene expression by the P[Asp(DET)] polyplexes (*N/P*=10 and 20) and PEG-*b*-P[Asp(DET)] polyplex micelles (*N/P*=10, 20, and 40), which showed successful transfection to MCTS, was quantified in this manner at each day period, and the results are shown in Fig. 6B. For both the polyplexes and polyplex micelles, increased the *N/P* ratios led to increased total intensities. Moreover P[Asp(DET)] polyplexes apparently had higher total intensities than PEG-*b*-P[Asp(DET)] polyplex micelles. The total intensity peaked at 6 days after transfection for all the polyplexes and polyplex micelles. It should be noted that such prolonged gene

expression is difficult to detect by the conventional monolayer culture study, because the monolayer cultured cells become confluent until 4 days, beyond which cell viability decreases remarkably. We also evaluated the relative intensity (=total intensity/volume of spheroid) of the expressed *Venus* in the spheroids transfected with the polyplexes or polyplex micelles (Fig. 6C) to normalize the differences in the growth rate and eventually the volume of each spheroid. Although the relative intensity of P[Asp(DET)] polyplexes decreased continuously with time, PEG-*b*-P[Asp(DET)] polyplex micelles with *N/P* ratios of 20 and 40 showed increased relative intensities until 4 days after transfection.

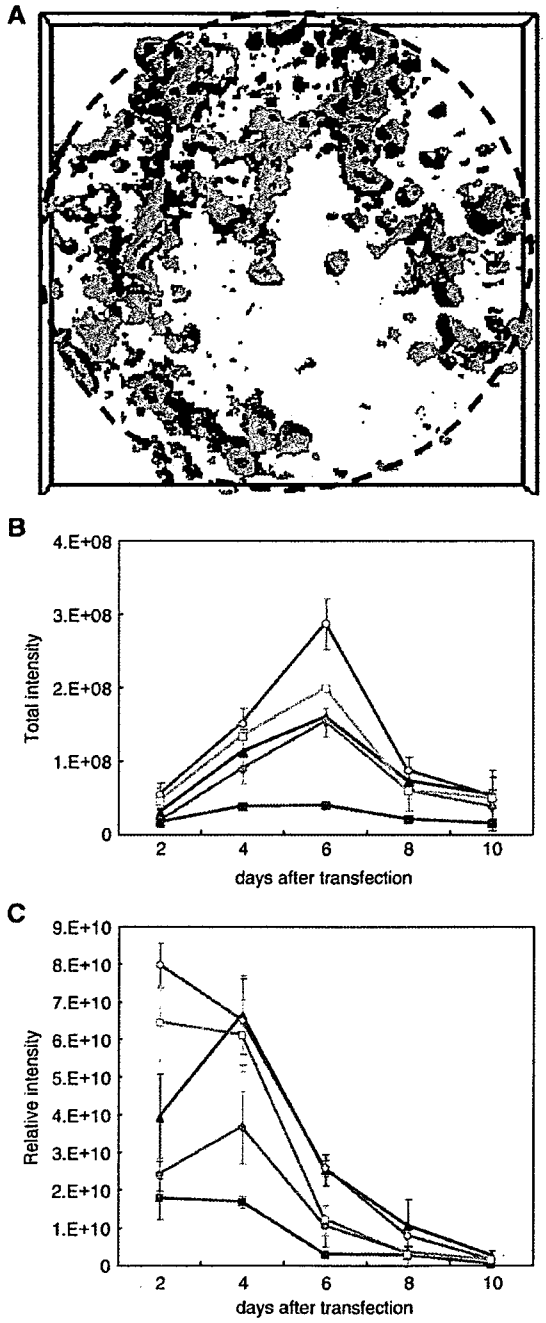

Fig. 6. Quantitative results of transfected fluorescent protein *Venus* in MCTS. A) Piled up images of transfected protein *Venus* from each slice by Imaris® (Carl Zeiss). B) Day-course of the change in total intensity by transfection with P[Asp(DET)] polyplexes (□; *N/P*=10, ○; *N/P*=20) and PEG-*b*-P[Asp(DET)] polyplex micelles (■; *N/P*=10, ●; *N/P*=20, ▲; *N/P*=40). C) Relative intensity (=total intensity/volume of spheroid) of fluorescence from transfected protein *Venus* with P[Asp(DET)] polyplexes (□; *N/P*=10, □; *N/P*=20) and PEG-*b*-P[Asp(DET)] polyplex micelles (■; *N/P*=10, ●; *N/P*=20, ▲; *N/P*=40).

3.6. DOPS-induced destabilization of P[Asp(DET)] polyplex and PEG-b-P[Asp(DET)] micelle

The differences in the time-dependency of the gene expression evaluated from the relative fluorescent intensity between P[Asp(DET)] polyplexes and PEG-*b*-P[Asp(DET)] micelles in Fig. 6C may reflect the differences in their behaviors after the internalization into the cell, because the transfection medium was replaced with fresh medium without polyplexes or micelles after 24 h. We therefore hypothesized that PEG-*b*-P[Asp(DET)] micelles may have greater stability or tolerability against pDNA unpacking, which is presumably induced through the exchange reaction with anionic components in the intracellular compartments, than P[Asp(DET)] polyplexes, thereby showing delayed gene expression. Thus, we evaluated the stability of the polyplex and polyplex micelle in the presence of anionic lipids (DOPS) as natural anionic compounds. It is known that such anionic lipids including phosphatidylserine exist appreciably in the intracellular compartments. As shown in Fig. 7, P[Asp(DET)] polyplexes (*N/P*=20) released pDNA at the [carboxyl groups in DOPS]/[phosphate groups in pDNA] (A/P) ratio of 12, whereas PEG-*b*-P[Asp(DET)] micelles (*N/P*=20) showed no pDNA release even at the highest *A/P* ratio (~17). Thus, PEG-*b*-P[Asp(DET)] micelles were judged to have higher tolerability against DOPS-induced destabilization than P[Asp(DET)] polyplexes.

4. Discussion

In this study, we prepared sets of cationic poly(*N*-substituted asparagine) homopolymers and PEG-*b*-poly(*N*-substituted asparagine) copolymers having the *N*-(2-aminoethyl)-2-aminoethyl group (P[Asp(DET)]) or *N*-(3-aminopropyl)-3-aminopropyl group (P[Asp(DPT)]) in the side chain (Scheme 1) to form polyplex-type non-viral gene vectors. To study the effects of the chemical structures of polycations and the effects of PEGylation of polycations on the properties as non-viral vectors, we carried out gene transfection to HuH-7 cells in the forms of monolayer culture and MCTS.

The in vitro evaluation of non-viral gene vectors relies mostly on the transfection study against monolayer cultured cells. However, there appear to be significant discrepancies between the environments of monolayer culture and in vivo tissues. One of these discrepancies is the short observable terms of the conventional monolayer cultures, which might prevent the study of the time-dependent properties of the gene expression of non-viral vectors. Especially for the polymeric gene delivery systems (polyplexes), in which pDNA is substantially condensed by